3-D CRUSTAL STRUCTURE OF THE ISPARTA ANGLE REGION FROM LOCAL EARTHQUAKE TOMOGRAPHY

by

Ersin Çakır

B.S., Geophysical Engineering, Çanakkale Onsekiz Mart University, 2007

Submitted to the Kandilli Observatory and Earthquake

Research Institute in partial fulfillment of

the requirements for the degree of

Master of Science

Graduate Program in Geophysics Department

Boğaziçi University

2011

3-D CRUSTAL STRUCTURE OF THE ISPARTA ANGLE REGION FROM LOCAL EARTHQUAKE TOMOGRAPHY

APPROVED BY:

Prof. Niyazi Türkelli . . . . . .

(Thesis Supervisor)

Prof. Hayrullah Karabulut . . . . . .

Prof. Aysun Güney . . . . . .

(Istanbul Technical University)

DATE OF APPROVAL:

ACKNOWLEDGEMENTS

I would like to thank Professor Niyazi Türkelli for his guidance, enlightening support and useful suggestions during my thesis. I would not able to complete this study without his help.

I also would like to thank Uğur Mustafa Teoman for helping me to employ 1-D and 3-D P-wave velocity inversion process. I am appreciated to Metin Kahraman for helping me in all steps of my thesis study. I am also appreciated to Didem Cambaz for helping me to write this work.

Also, I would like to thank Ekrem Zor and Adil Tarancıoğlu for their helpful guidance to employ 1-D P-wave velocity inversion process.

I would like to acknowledge my family and my fiancée Derya Yaman who never left me alone when I come across a difficulty.

This research is supported by Boğaziçi University Research Fund (Grant No. 07T203).

ABSTRACT

3-D CRUSTAL STRUCTURE OF THE ISPARTA ANGLE REGION FROM LOCAL EARTHQUAKE TOMOGRAPHY

Isparta Angle is a seismically active and complex zone in terms of tectonic and geologic features. A temporary seismic network consisting of nineteen three-component broadband stations were installed around Isparta Angle (IA) and surroundings to address some of the important questions. Detailed crustal structure of the Isparta Angle were obtained using the seismic data collected over two years from July 2006 to June 2008. Results of this study will contribute to beter characterize the crustal structure and the seismicity of the region.

In this study, local earthquake data that were collected from temporary broad-band seismic array operated in the region, data from permanent stations of Kandilli Observatory and Earthquake Research Institute (KOERI), permanent stations of Disaster and Emergency Management Presidency (DEMP) and Süleyman Demirel University (SDU) in order to determine the upper crust seismic P wave velocity structure of IA and the surrounding regions by three-dimensional (3-D) Local Earthquake Tomography (LET) method. S-wave arrival times were not included due to strong attenuation and higher picking errors of S-phases.

The result of tomographic processes, 3-D velocity model, was compared with the seismological and tectonic features of the region and also compared with the results of the previous studies in the region. The results suggest that low-velocity zones beneath Isparta Angle in the depth range between 0-10 km can be related to alluvial deposits, and the velocity variation below 20 km depth can be related with the transition from upper crust to lower crust.

ÖZET

ISPARTA BÜKLÜMÜNÜN 3 BOYUTLU SİSMİK HIZ YAPISININ YEREL DEPREM TOMOGRAFİSİ YÖNTEMİYLE ARAŞTIRILMASI

Isparta büklümü, tektonik ve jeolojik özellikleri bakımından sismik olarak aktif ve karmaşık bir yapıya sahiptir. Bu anlamda önemli soruların cevaplanabilmesi için Isparta büklümü ve çevresinde ondokuz istasyondan oluşan geçici bir sismik ağ kurulmuştur. Temmuz 2006-Haziran 2008 arasında toplanan sismik verinin işlenmesiyle, bölgenin kabuk yapısı hakkında detaylı ve hızlı bilgiler elde edilmiştir. Bu çalışmanın sonuçları bölgenin güncel sismik aktivitesi ve kabuk yapısını anlama konusunda kayda değer faydalar sağlamaktadır.

Bu çalışma kapsamında, Isparta büklümü ve çevresinin üst kabuk yapısının P dalga hızı modelini 3 Boyutlu Yerel Deprem Tomografisi yöntemi ile araştırmak için bölgede geçici olarak kurulmuş olan geniş bantlı sismik istasyonlardan, Kandilli Rasathanesi ve Deprem Araştırma Enstitüsü'nün, Afet ve Acil Durum Yönetimi Başkanlığı'nın ve Süleyman Demirel Üniversitesi'nin bölgedeki sabit istasyonlarından alınan sismik veriler kullanılmıştır. Bu yöntemde çözünürlük kavramı çok önemli olduğundan, P fazı okumalarına göre daha fazla hata içeren ve hızlı bir şekilde sönüme uğrayan ve yine P fazı okumalarına göre daha az sayıda olan S fazı okumaları işleme sokulmamıştır.

Özetle, tomografik işlemler sonucunda elde edilen 3 boyutlu P dalga hız yapısı bölgenin sismolojik ve tektonik yapısı ile ilişkilendirilmiştir. Elde edilen hız yapısı ve özellikleri bölgede daha önce yapılmış olan araştırmaların sonuçları ile de karşılaştırılmıştır. Çalışmanın sonuçları, ilk 10 km derinlikteki düşük hız zonlarının alüvyon yığışımları olarak, yaklaşık 20 km derinlikteki hız artışının da üst kabuk – alt kabuk sınırı olabileceğini ortaya koymuştur.

TABLE OF CONTENTS

LIST OF FIGURES

LIST OF TABLES

LIST OF ABBREVIATIONS

IA	Isparta Angle
ACH	Aki-Christoffersson-Huseybe
WAEP	Western Anatolia Extensional Province
GPS	Global Positioning System
LET	Local Earthquake Tomography
KOERI	Boğaziçi University Kandilli Observatory and Earthquake Research Institute
SDU	Süleyman Demirel University
DEMP	Disaster and Emergency Management Presidency
RMS	Root Mean Square
BVP	Boundry value problem
IVP	Initial value problem
SVD	Singular Value Decomposition
Vp	P-wave Velocity
FBFZ	Fethiye-Burdur-Fault-Zone
SF	Sultandağ Fault
RDE	Resolution Diagonal Element
DWS	Derivative Weighted Sum
ART	Algebraic Reconstruction Technique
SIRT	Simultaneous Iterative Reconstruction Technique
WAEP	Western Anatolia Extensional Province
KHIT	Ray Hitcount

1. INTRODUCTION

In this research three-dimensional (3-D) velocity structure of the upper crust of the Isparta Angle (IA) and surroundings was determined in a local scale by using one-dimensional (1-D) velocity inversions and three-dimensional (3-D) tomographic inversion techniques. For this purpose, a seismic data set were combined from the temporary seismic network consisting of 19 three-component broadband stations which were operated in and around the Isparta Angle region from August 2006 to November 2009 and also from the Kandilli Observatory and Earthquake Research Institute (KOERI) permanent broad band seismic stations in the region. The three-year field experiment was aimed to collect a high quality data set that would allow us to apply different seismic methodologies to enhance our knowledge of the evaluation and the seismic regime of the Isparta Angle. The parts of earthquake data from July 2006 to June 2008 were included in this study. This work demonstrates that resulting 3-D P-wave velocity model leads to a better seismotectonic analysis of this tectonically and structurally complex region. Resulting 3-D model can also help to delineate crustal deformation patterns within the crust which have an important broader impact in terms of seismic hazard in the region.

The Isparta Angle (IA) is located in southwestern Turkey as an intersection of the Hellenic and Cyprian Arcs. The region has been subjected large devastating earthquakes such as the 2001 Sultandağ Earthquake (Ms 6.4) and the 1971 Burdur Earthquake (Ms 5.9), associated with fault zones such as Fethiye-Burdur-Fault-Zone and Sultandağ Fault. In addition, wide variety of tectonics has also created a complex upper mantle and crustal structure that affects regional wave propagation both in terms of amplitude and travel times, and also seismic anisotropy.

The seismic tomography method applied to the study of the Earth's interior was devoloped from the mid-1970s (Aki *et al.,* 1976) which is based on the time residuals of seismic wave arrivals with respect to those expected from an initial model (Udias, 1999). The method permits the deduction of the three dimensional models of inhomogenities in the Earth's interior from the crust to the nucleus.

The first 3-D inversion method, the Aki-Christoffersson-Huseybe (ACH) method (Aki *et al.,* 1977), was the first application of tomography in seismology and has by now been used by seismologists to image the three-dimensional structure of the crust and upper mantle for so many regions in the Earth.

Seismic tomography depends on the presence of contrast in seismic properties. Such differences in three-dimensional structure are reflected directly in the arrival times of seismic phases or through the shape and amplitude of seismic waveforms. Today, highly resolved tomographic images are essential for variety of applications, ranging from global-scale geodynamics such as earthquake location procedure to local-scale engineering such as settlement plan for cities. There are two general strategies to improve seismic tomography: 1) to develop more elaborate modeling and inversion techniques, such as finite-frequency tomography (i.e., Yoshizawa and Kennett, (2004)) or nonlinear full-waveform inversion (i.e., Fichtner *et al.,* 2008) and 2) to incorporate previously unexploited data such as surface-wave amplitudes, exotic phases, and measurements of seismically induced strain (i.e., Mikumo and Aki, 1964) or rotations (Bernauer *et al.,* 2009).

Within a few years after the application of Aki, the tomography method applied to data from 25 arrays around the world apertures ranging from 20 to 3000 km. Hirahara (1977) investigated the upper mantle under Japan delineated the subducing high velocity Pacific plate using this method. However, important improvements to the original technique were implemented by Pavlis and Booker (1980) who introduced the seperation of parameters technique, allowing the analysis of the large data sets. In the mid-1980s, iterative matrix solvers were implemented by Clayton and Comer (1983) and Nolet (1985) causing a jump in the number of model parameters.

In global scale, application of a similar method to ACH was performed by Dziewonski and Anderson (1981) and Sengupta and Toksöz (1976). Dziewonski and Anderson described the results of 3-D analyses of mantle structure obtained by research groups at Harvard and Caltech. Because of the similarity of the medical x-ray tomography, which yields images of specific plane sections of the body, they called the techniques of mapping the 3-D structure of earth's seismic tomography. Sengupta and Toksöz (1976)

obtained 3-D velocity models for the earth's mantle satisfying P, S, PcP and ScS traveltime anomalies from deep focus earthquakes.

In local scale, different types of forward solvers (ray tracing schemas) have become a significant part of the Local Earthquake Tomography-LET applications. Um and Thurber (1987) developed more accurate bending ray tracers finite difference and shooting (Runga Kutta Perturbations) ray tracers were implemented in tomographic studies (Virieux and Arra, 1991). Husen *et al.,* (2000) constructed the 3-D image of the subduction zone in north Chile. More recently, Zhao *et al.,* (2005) determined a detailed tomographic image of the crust in the 1992 Landers Earthquake (M 7.3) region in southern California, Yang and Shen (2005) developed a 3-D P-wave velocity model of the Icelandic crust and uppermost mantle from tomographic inversion of over 3500 first-arrivals from local earthquakes recorded in Iceland. As far as Isparta Angle and surroundings concerned, 1-D crustal model of the western Anatolia has been obtained by teleseismic inversion method (Erduran, 2009). Researchers have found that the shear wave velocity increases from 2.5 km/s to 3.0 km/s in the first 5 km. Below this, there is a velocity jump at about 10 km, velocities has a positive gradient from 3.0 km/s to 3.2 km/s.

Seismic tomography can be classified through the tomographic methods by the distribution type of sources and receivers, by whether the whole ray or only part of its model, by the type of data used, by the type of error minimization (generally least-squares), by a priori constraints and by the type of inversion.

Classification in terms of source:

a) Earthquake tomography: Natural sources, earthquakes, are used in this tomography method. Hypocenter-velocity coupling becomes the important part of the problem due to the unknown hypocentral parameters (latitude, longitude and depth) and origin time of the earthquakes used. This problem requires relocation of earthquakes during inversion process.

b) Controlled source tomography: Man-made events such as shots or blasts are used in controlled source tomography. The best advantage of this method is to know exact

hypocentral parameters and time of the event that is the opposite case in the earthquake tomography. Therefore, this method does not require relocation or any additional process. Because the source parameters are known, hypocenter-velocity structure coupling is not a problem for this method. High frequency seismic receivers such as geophones are used in this method.

Classification in terms of source-receiver geometry:

a) Local earthquake tomography (LET): The structure of upper crust is resolved in a local scale in LET method. The observed phases are mostly the direct arrivals (Pg, Sg). The events used must occur in a volume of the medium that is interested and be measured by a homogeneous and dense network. The phase quality and network density are important factors for LET to work properly.

Moreover, the major LET applications were performed by Kissling (1988) and Thurber (1993) so useful information about the process steps and details of LET method from their research could be taken as an example. LET comprises the inversion of travel times, recorded locally, for Vp and Vs velocities or Vp/Vs ratios. Model parameters are changed to minimize the difference between observed and calculated travel times (residuals) in least square sense. Synthetic travel times are calculated using mostly ray tracing methods. Further information about LET will be given in Chapter 5.

b) Teleseismic Tomography: Resolution in teleseismic tomography of upper-mantle structure depends critically on our understanding of the 3-D crustal velocity structure beneath a receiver array. Because of the low frequencies and near-vertical angle of incidence of incoming waves, teleseismic traveltime tomography resolves the crustal-scale structure poorly, though complex crustal structures influence teleseismic traveltimes strongly (Waldhauser *et al.*, 2002). Long-period (T > 30) seismic signals recorded at a densely spaced seismic array signals instead of direct arrivals those are used in local tomography are used in teleseismic tomography to determine velocity structure of whole earth in a spherical space. Data are provided by international and local networks around the globe.

Earthquakes are located at great distances stations (generally > 2500 km) from a localized cluster of seismic stations for teleseismic tomography. With this geometry, the wave's incident on the array can be treated as plane waves.

There are also other tomography methods such as Full 3-D Tomography (Chen *et al.*, 2007a, b) referred as series expansion methods. These methods start by considering the object or area of interest to be compromised of boxes or pixels. Energy is considered to propagate through the various pixels to provide a sum or projection of the pixel values. The pixel values are now correlated to sum. A stable but approximate solution, as discussed above is known as backprojection corresponds to using the transpose of matrix instead of inverse. Two other more accurate but iterative methods are known as ART (Algebraic Reconstruction Technique) and SIRT (Simultaneous Iterative Reconstruction Technique), however these techniques require high-tech computers and parallel computing technology (Chen *et al.*, 2007a,b).

Following the general terms about seismic tomography, tectonic setting of Isparta Angle and surroundings were given in section 3 by the previous studies for the region.

In Chapter 4, derivation of the 1-D minimum P wave velocity model (which serves as an initial model for the tomographic inversion) was presented in quite detail along with the theory and calculation steps. Depending on a certain criteria, proper data selection was made for the 1-D simultaneous velocity inversion via VELEST algorithm with several trial velocity models (with certain number of iterations) and the final event locations are shown. Residuals and rms errors calculated using initial and 1-D minimum model was compared in order to check stability of the obtained model.

In Chapter 5, LET method and its implications to derivate 3-D P wave velocity model were extensively explained.

In Chapter 6, detailed information about tomographic inversion that was performed by using SIMULPS14 is given. Two resolution tests were performed in order to prove solution quality and resolve power of the resulting 3-D P wave velocity model. Parameters those are used in SIMULPS14, resolution test results and tomographic inversion results are

mapped in different cross-sections that are shown in the map together with the updated hypocenter locations.

Conclusions that are based on the overall tomographic results are explained and interpreted from a tectonic point of view in Chapter 7.

2. TECTONIC STRUCTURE AND PREVIOUS STUDIES

2.1. Overview of the Tectonic Structure of Isparta Angle and Surroundings

The Isparta Angle (IA) is located in southwestern Turkey as a convex intersection of the Hellenic and Cyprian Arcs related to the collosion of the African and Anatolian plates and possesses a complex future. Figure 2.1 illustrates the Geodynamic framework of the Eastern Mediterranean that the IA is formed along the boundry of African and Eurasian plates by NE- and NW-striking faults north of the Antalya Gulf in south-western Turkey, NE-striking Fethiye-Burdur Fault Zone bounds the IA to the west (Dumont *et al.,* 1979; Price and Scott, 1994; Yağmurlu *et al.,* 1997) and NW-striking Akşehir fault bounds the IA to the east (Yağmurlu *et al.,* 1997). The northern tip of IA defines the boundry between Western Anatolia Extensional Province (WAEP) and the Central Anatolia Province (Barka and Reilinger, 1997; Glover and Robertson, 1998; Bozkurt, 2001). IA, a weak transtensional future dominated by right-lateral strike-slip faulting, separetes a western Anatolian-Aegean extensional domain from the eastern Anatolia (Glover and Robertson, 1998). According to this view, IA expresses north-south slab-tearing associated with post-collosion subduction (Çoban and Flower, 2006). An alternative model views the faulting as predominantly left-lateral, allowing for differential motion between the Hellenic and Cyprus arcs (Barka and Reilenger, 1997).

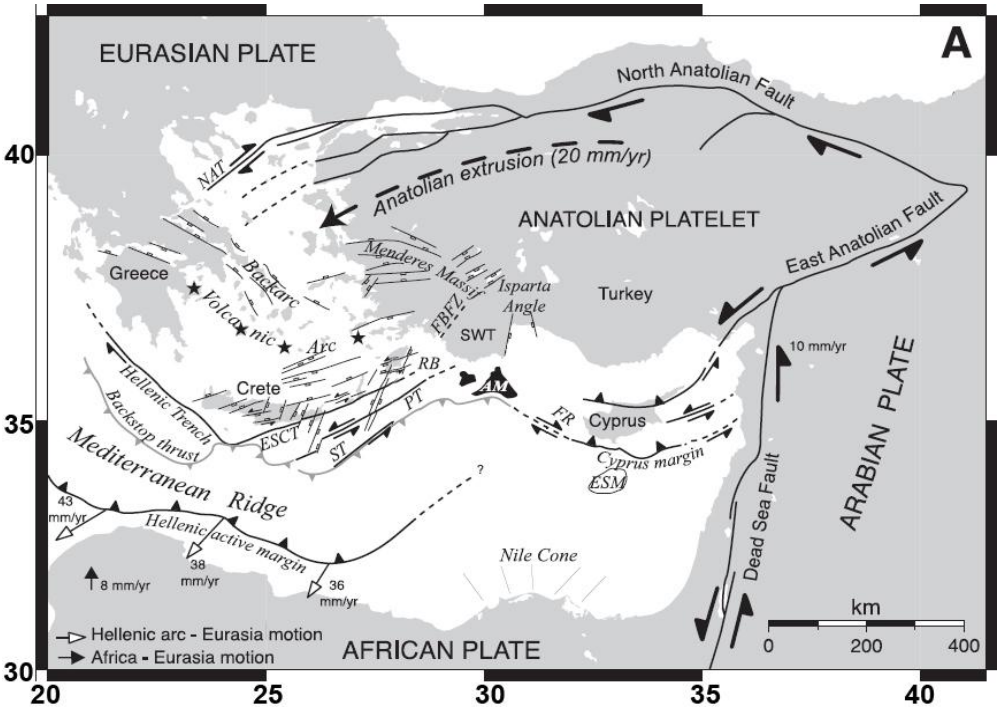

Figure 2.1. Geodynamic framework of the Eastern Mediterranean (After Veen, 2004)

In Figure 2.1, ESCT denotes East South Cretan Trough, ST deotes Strabo Trench, PT denotes Pliny Trench, RB denotes Rhodes Basin, AM denotes Anaximander Mountains, FR denotes Florence Rise, ESM denotes Erastothenes Seamount, FBFZ denotes the hypothetical Fethiye–Burdur Fault Zone, SWT denotes Southwest Turkey, NAT denotes North Aegean Trough (Veen, 2004).

GPS measurements revealed that the Arabian plate moves northward with respect to the Eurasia at a rate of 23 +- 1 mm/yr, 10 mm/yr of this rate (Figure 2.2) is taken up by shortening in the Caucaus (Barka and Reilinger, 1997). The movement of the Arabian plate is concluded with collision that caused westward displacement and counterclockwise rotation of the Anatolian block (McKenzie, 1972) that could be related to extension of Aegean.

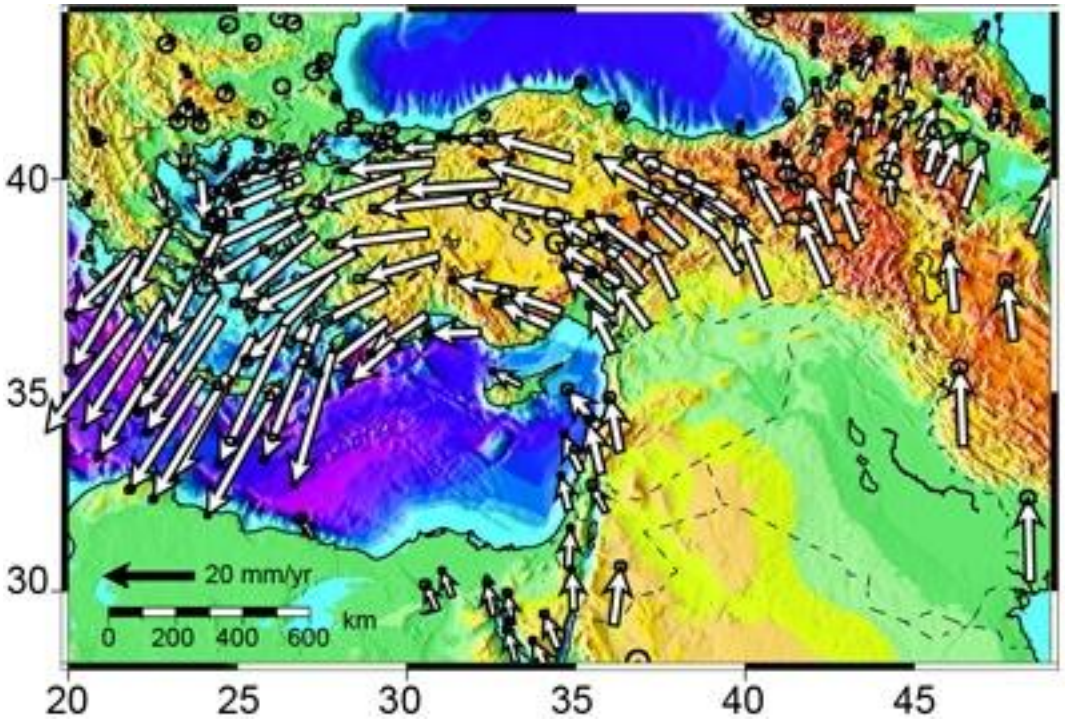

Figure 2.2. Map showing decimated GPS velocities relative to Eurasia (After Reilinger, 2006)

On the other hand, African Plate moves northward with respect to Eurasia at a rate of ~10 mm/yr (Reilinger, 2006). So the displacement of the African plate is resulted in subduction of African plate underneath the Aegean plate and therefore is related to the slab pull which is the other debate about the extension of the Aegean (McKenzie, 1978; LePichon and Angelier, 1979). Western part of Anatolian Plate moves to the westward with respect to Eurasia at a rate of ~20 mm/yr, however this rate increases about 5-10 mm/yr to the west-southern part of Anatolian Plate. Within this tectonic framework, IA constitutes the junction between the Cyprus and Hellenic arcs and is a tectonic assembles which has a complex tectonic history (Barka and Reilinger, 1997).

There are two different fundamental hypotheses for the tectonic framework of the region. Glover and Robertson (1998) suggested that the Isparta Angle is dominated by right lateral strike slip fault systems. The Isparta Angle is bounded by Burdur fault which indicates oblique fault mechanism with right lateral and normal displacements. They also suggested that the eastern side of Isparta Angle is bounded by right lateral fault systems. Within these fault systems Isparta Angle is an extensional system between the rotating

blocks of western and eastern Anatolia. According to Glower and Robertson (1998) a slab tear might localize the weak zone between western and eastern Anatolia in north-south direction.

However, Barka and Reilinger (1997) suggested that the region is dominated by left lateral strike slip fault systems. So western tip of Isparta Angle is bounded by Burdur fault which indicates left-lateral displacements and acts as an accommodation zone between Hellenic and Cyprus arc systems and Burdur fault is mainly responsible for slab tearing between the Hellenic and Cyprus arc systems. There are two different view about the tectonic frame of the region, however there is a common point of these two views: there is a slab tearing between western and eastern Anatolia.

The distribution of earthquake epicenter locations, b-values, and interpretations of gravity data suggest the presence of a subduction zone in the area extending from the western part of the Cyprian arc to the Isparta Angle area including Antalya Bay (Kalyoncuoğlu *et al.*, 2010).

Based on tomographic images, Facenna *et al.,* (2006) suggested that deep slab is detached from its upper portion beneath the Bitlis-Zagros collisional belt and that the rupture can be prolonged to the west at least till Cyprus and probably till the Hellenic trench. For the eastern side of the Cyprus, slab-break off likely occurred, but the western Cyprus arc is still connected to the slab (Kalyoncuoğlu *et al.,* 2010).

2.2. Previous Studies in Isparta Angle and Surroundings

Isparta Angle and surroundings are active regions in terms of seismicity, so crustal structures of the Isparta Angle have been extensively investigated in many studies.

Kalyoncuoğlu and Özer (2003) have observed that the crustal models suggest the crust consist of three distinct layers from receiver function analysis beneath the Isparta broadband seismic station. The surface layer is 2 km thick and S-wave velocity is about 2 km/s, the second is 15 km thick and S-wave velocity is about 3.35 km/s. The third layer shows S-wave velocity of about 3.8 km/s and is 14 km thick. The Mohorovicic

discontinuity beneath the ISP station indicates P-wave velocity is around 8.0±0.2 km/s, S-wave velocity 4.5±0.1 km/s and upper mantle depth is 31±1 km.

Al-Lazki *et al.,* (2004) have observed that localized anisotropy orientations are underlined by very low Pn velocity zones (Pn < 7.8 km/s) such as northern Aegean zone and the Isparta Angle. They have suggested that there is a complex process including crustal and upper mantle deformation beneath the Arabian plate. The results of Pn tomography study (Al-Lazki *et al.,* 2004) have indicated that the fast axis direction of the upper mantle anisotropy beneath the Isparta Angle is approximately N–S.

Sapaş and Boztepe-Güney (2008) have suggested a two-layer anisotropic model with a horizontal symmetry axis for mantle anisotropy beneath the Isparta Angle consisting of 'frozen-in' anisotropy in the upper mantle (φu = 150.0˚, δtu = 1.6 s) and anisotropy caused by the asthenospheric flow (φl = 40.0◦, δtl = 1.0 s) and the crust is also under the effect of stress regime in the direction of NE–SW similar to asthenospheric flow. They conclude that the backazimuthal variations of the splitting parameters at ISP station indicate a different and complex mantle polarization anisotropy for the Isparta Angle in southwestern Turkey compared to those obtained for ANTO and ISK stations.

Erduran (2009) has found that the shear wave velocity increases from 2.5 km/s to 3.0 km/s in the first 5 km from teleseismic inversion method. Below this, there is a velocity jump at about 10 km, velocities has a positive gradient from 3.0 km/s to 3.2 km/s. Although following 10 km has a constant velocity, there is a low velocity zone at about 20 km, velocity reduces from 3.40 km/s to 3.20 km/s. Researcher has also found that Moho discontinuity at about 40 km and has a shear velocity of 4.4 km/s. Similarly, these low velocity zones were also interpreted as recent volcanism.

Poyraz (2009) has observed that crustal thickness below the ISP station, is about 31-35 km and a decrease in S-wave velocity for 60-70 km depth; Dilek and Altunkaynak (2009) relate this low S-wave velocty with a shallower astenosphere. Similarly, Kahraman (2008) has also observed the crustal thickness beneath the ISP station is about 35.7-37.5 km. Poyraz (2009) has also observed that there is a radial expanding from the focal mechanism analysis of the 2000 Sultandağ Earthquake and the 1971 Burdur Earthquake.

Kahraman *et al.,* (2010) found that average mid crustal shear velocity is 3.49 km/s however the mid crustal velocities directly above IA is ranging between 3.47 km/s and 3.53 km/s and the average upper mantle P-wave velocity is 7.53 km/s from joint inversion of P-wave receiver function analysis. They have also found that region has crustal thickness varies from 26-34 km.

Tezel *et al.,* (2010) have observed low velocity layers beneath some stations from receiver function analysis and interpreted these low velocity layers as partial melting of a young and hot subducted structure in the region, also they have observed some mid-crustal discontinuities at 10-15 km, they have observed Moho discontinuities at 25-35 km and 20-25 km respectively. Shear wave speed was found to vary between 3.3 km/s and 3.7 km/s in the lower crust and between 4.1 km/s and 4.4 km/s uppermost mantle and the Moho depth is increasing from western Anatolia to central Anatolia considering inversion results and 2-D depth-migrated receiver functions.

Cambaz and Karabulut (2010) have found that the IA is marked by a wedge-shaped low group velocity anomaly that is related to crustal thickening and subduction-related complex from Love-wave group velocity study.

The study "Geophysical and geological imprints of southern Neotethyan subduction between Cyprus and the Isparta Angle" was performed in the region by Kalyoncuoğlu *et al.,* (2010).

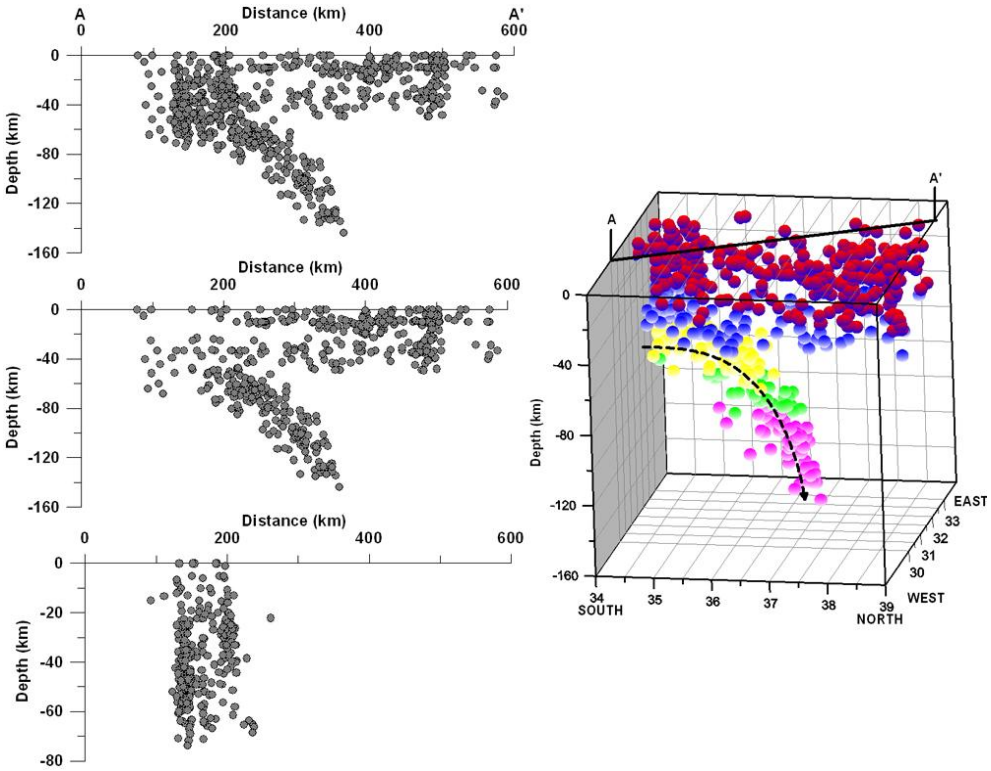

Figure 2.3. Map showing earthquake epicenters in terms of depth and distance (Kalyoncuoğlu *et al.*, 2010)

Researchers have analyzed epicenter distribution of earthquakes (Figure 2.3), b-values (Table 2.1) and gravity anomalies for 5 depth intervals (0-35 km, 35-55 km, 55-75 km, 75-95 km, >95 km) on NE-SW trending regional profiles and compared with geological structures in order to understand plate interactions within the area between Isparta Angle and Cyprus arc. The results of this study suggest the presence of subduction zone inclined to the northeast beneath the eastern limb of the Isparta Angle for the area between the apex of Isparta Angle and the western Cyprian arc by taking into consideration the distribution of earthquake epicenter locations, b-values, and gravity data.

Table 2.1. The results of b-value maps (Kalyoncuoğlu *et al.*, 2010)

Depth interval (km)	bmin	bavr	bmax
0-35	0.60	0.80	0.97
35-55	0.52	0.66	0.77
55-75	0.88	1.0	1.2
75-95	0.72	0.85	0.98
95<	0.63	0.75	0.87

Biryol *et al.,* (2011) have observed a crustal model which suggests that, the inferred gentle dip of the western Cyprus slab at shallow depths (<60 km) beneath Isparta Angle is related to subduction of a locally thicker continental fragment of the African margin from teleseismic *P*-wave traveltime tomography. This is also supported by the presence of intermediate depth seismicity (70–120 km deep) in this region. This continental fragment may have obstructed the subduction near the Isparta Angle and slowed the westward motion of southern Anatolia.

Overall, studies performed in the region suggested that Mohorovic discontinuity is at about 35-40 km depth with 4.0-4.4 km/s shear velocity. There are some low velocity zones at about 15-20 km depth, and all of the studies suggest that these low velocity zones indicate recent volcanism. Furthermore, there is a velocity jump at about 10 km depth.

3. SEISMIC EXPERIMENT AND DATA

A 19 station broadband array was operated from August 2006 to November 2009 and over 300 Gigabytes of data were collected to assess the crustal and upper mantle structure and dynamics of the IA and surroundings. Part of the data for time period from July 2006 to June 2008 used in this research. In addition to the KOERI, the Disaster and Emergengy Management Presidency (DEMP) and the Suleyman Demirel University (SDU) permanent broad band seismic stations in the region and University of Missouri also supported this research by 9 seismic stations for one year. Distribution of the seismic stations is shown in Figure 3.1. Broad-band data were recorded continuously at 50 sps (samples per second) which provided high enough sampling for accurate event locations. The spacing between stations was about 30-40 km.

This work demonstrates that improved earthquake locations computed in a 3-D velocity model lead to a better seismotectonic analysis of this very complex region. Earthquake event locations can also help to delineate crustal deformational patterns within the crust, which has an important impact in terms of seismic hazard to the many people living in the region.

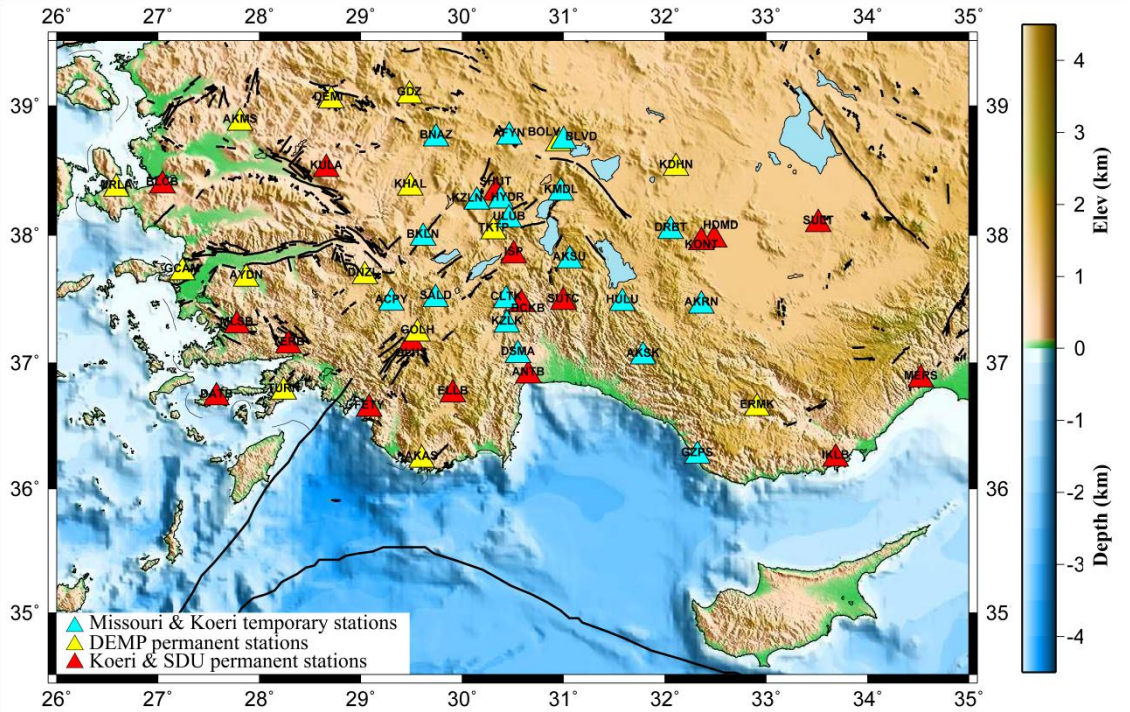

Figure 3.1. The station geometry for Isparta project. Blue triangles denote temporary stations, red triangles denote DEMP's permanent stations, and green triangles denote KOERI & SDU permanent stations.

The data were prepared according to KOERI event list that is from July 2006 to June 2008. That list includes events which have the magnitude above 3, and events that occurred within the region shown in Figure 3.1.

3.1. Initial Earthquake Locations

The first step of seismic tomography is to obtain earthquake locations with a priori 1-D model and then obtain “minimum 1-D model” by using these earthquake locations and trial crustal models in order to use in Local Earthquake Tomography (LET).

P and S phases were picked from 1347 events. These phases were weighted between 0-4, in this case 0 is the best pick, 4 is the worst pick. We used HYPOCENTER (Lienert and Haskov, 1995) software to locate the events. A total of 875 events were located out of 1347 events by using priori 1-D model that is KOERI‘s generalized model for Turkey (Table 3.1). Figure 3.2 depicts initially located events.

Table 3.1. Initial 1-D velocity Model

	P-wave Velocity (km/s)	**Depth (km)**
Layer 1	4.50	0.00
Layer 2	5.91	5.40
Layer 3	7.80	31.60
Layer 4	8.30	89.20

Events with azimutal gaps from 49 to 349 (158 degrees mean) were located initially in the period from July 2006 to June 2008. Root mean square (RMS) values for these events were between -1 and +1, and mean RMS value was 0.5. During this time period ten moderate size earthquakes occured in the region which are posted in Table 3.2.

Table 3.2. Moderate size earthquakes occured between July 2006 and June 2008

No	**Date (Day, Month, Year)**	**Time (Hour, Min, Sec)**	**Magnitude**	**Latitude (˚)**	**Longitude (˚)**	**Depth (km)**
1	23.01.2007	21.21.57	Ml 4.5	38.12	28.75	3
2	15.02.2007	03.15.53	Mb 4.1	36.08	28.00	86
3	30.03.2007	16.56.53	Ml 4.8	38.00	30.92	6
4	30.03.2007	19.23.55	Ml 4.7	37.99	30.91	5
5	10.04.2007	21.39.18	Ml 4.7	38.01	30.95	7
6	10.04.2007	22.00.34	Ml 4.9	38.00	30.94	5
7	29.10.2007	09.23.14	Mb 4.9	37.01	29.25	1
8	31.10.2007	17.58.00	Ml 4.5	36.98	29.28	10
9	16.11.2007	09.08.22	Ml 5.0	37.02	29.26	5
10	02.12.2007	20.21.50	Mb 4.6	37.07	29.22	6

It has been observed that, our network is able to locate events within 2-3 km of the true epicenter and the hypocentral errors can not exceed 7 km for well located events even when not using an optimal velocity model. The horizontal and vertical locarion errors are between 4-6 km and 7-9 km respectively for the well-located events in the region. Figure 3.3 represents the flow chart of the process.

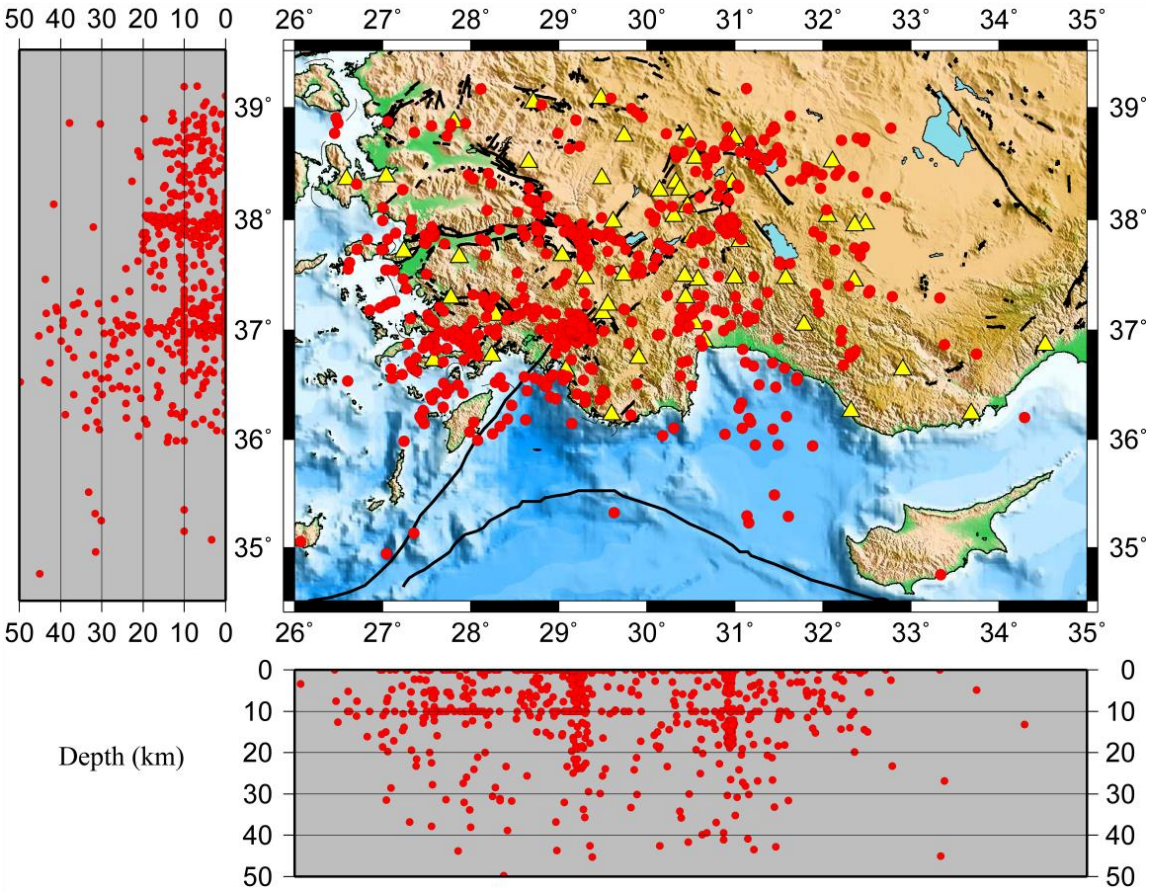

Figure 3.2. Initial earthquake locations and depth distribution along latitude and longitude. Yellow triangles represent the stations and red circles represent the events

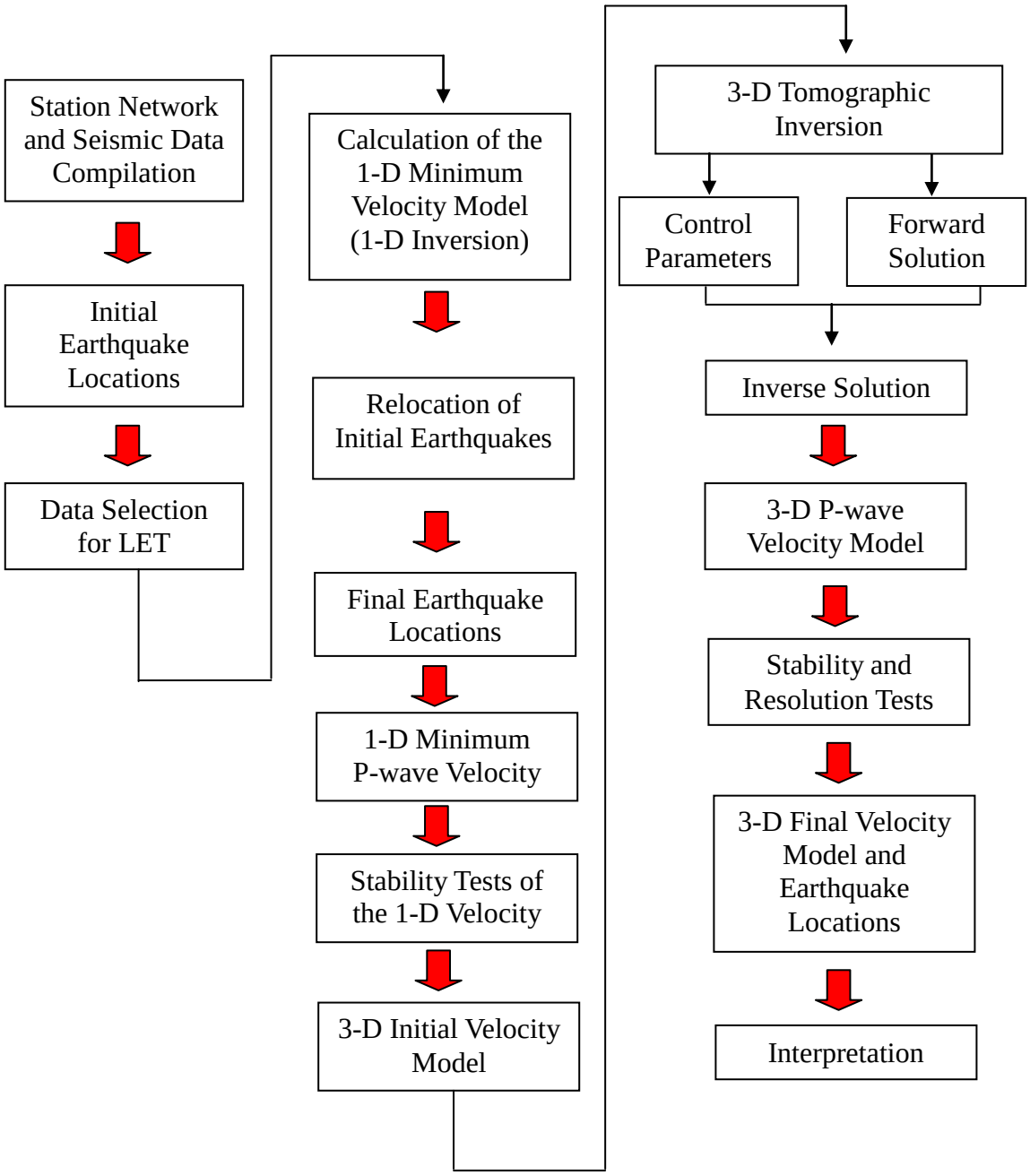

Figure 3.3. Flow chart of the calculation steps of the study

4. DERIVATION OF MINIMUM 1-D VELOCITY MODEL FOR LOCAL EARTHQUAKE TOMOGRAPHY (LET)

Two-step tomography process (Kissling *et al.,* 1994) was employed in order to determine the three-dimensional crustal velocity structure of the Isparta Angle and surroundings. Following Aki and Lee (1976) solutions are obtained by linearization with respect to a reference earth model, so inappropriate models may results in artifacts (Kissling *et al.,* 1994). Kissling *et al.,* (1994) proposed a procedure to obtain the best fittings 1-D initial model to overcome these problems.

The travel-time data are inverted jointly with revised hypocenter coordinates and station corrections to obtain a 1-D tomographic solution. This model is called the ‘‘minimum 1-D model’’ (Kissling, 1988). The determination of this model is a trial and error process that ideally starts with the collection and selection of a priori information about the subsurface structure. Since this process can lead to ambiguous results, particularly when more than one priori 1-D models have been established, several parameters which control the inversion must be varied and the corresponding results must be evaluated (Kissling *et al.,* 1994).

The coupled hypocenter-velocity problem, the derivation of the 1-D minimum velocity model for Isparta Angle and surroundings and data compilation for the simultaneous inversion will be explained in more detail in the following sections.

4.1. Coupled Hypocenter-Velocity Problem

Following Kissling *et al.,* (1994), the arrival time of a seismic wave generated by an earthquake is a non-linear function of the station coordinates (s), the hypocentral parameters (h) including origin time and geographic coordinates and the velocity field (m).

$$t_{obs} = f(s, h, m) \tag{4.1}$$

Using a priori 1-D velocity model, rays are traced from a trial source location to the receivers and calculate theoretical arrival times (t_{calc}). The difference between observed and calculated travel times is called the residual travel-time (t_{res}). The residual travel time can be expanded as functions of differences (Δ) between the estimated and the true hypocentral and velocity parameters. To calculate suitable corrections to the hypocentral and model parameters, the dependence of the observed travel times on all parameters should be known. A linear relationship between traveltime residual and adjustments to the hypocentral (Δh_k) and velocity (Δm_i) parameters are obtained:

$$t_{res} = t_{obs} - t_{calc} = \sum_{k=1,4} \frac{\partial f}{\partial h_k} \Delta h_k + \sum_{i=1,n} \frac{\partial f}{\partial m_i} \Delta m_i + e \tag{4.2}$$

This equation can be written in matrix notation as:

$$t = Hh + Mm + e = Ad + e \tag{4.3}$$

Equation 4.3 is so called the coupled hypocenter-velocity model problem where:

$\boldsymbol{t}$: Travel time residuals,
$\boldsymbol{H}$: Matrix of partial derivatives of travel time with respect to hypocentral parameters,
$\boldsymbol{h}$: Hypocentral adjustments,
$\boldsymbol{M}$: Partial derivatives of travel time with respect to model parameters,
$\boldsymbol{m}$: Model parameter adjustments,
$\boldsymbol{e}$: Travel time errors, including errors in measuring tres, errors in tcalc due to errors in station coordinates, use of the wrong velocity model and hypocentral coordinates, and errors caused by linear approximation.
$\boldsymbol{A}$: All partial derivatives
$\boldsymbol{d}$: Hypocentral and model parameter adjustments.

According to Thurber (1992) and Eberhart-Philips and Michael (1993) ignoring the effect of the term Hh in Equation 4.3 will introduce systematic errors into the estimated hypocenter during the location process.

4.2. Concept of the Minimum 1-D Velocity Model

Taking as an example of Kissling *et al.,* (1994) study the chances for successful estimation of the true velocity model using Equation 4.3 can obviously be improved by selecting a velocity model in the neighborhood of the true model so 1-D minimum velocity model is calculated and taken as an input model for 3-D seismic tomography. Kissling *et al.,* (1994) suggest that the natural starting point is the 1-D velocity model that itself represents the least squares solution to Equation 4.3.

Minimum 1-D P-wave velocity model is calculated through a trial-error process after collecting and selecting priori information about the crustal structures of the region. Kissling *et al.,* (1994) proved that several 1-D models may lead ambigious results especially if parameters that control the inversion are not varied. The results strongly depend on the proper data selection process.

In this study, calculation of minimum 1-D P-wave velocity model is performed by a FORTRAN code VELEST (Kissling *et al.,* 1994; Kissling *et al.,* 1995) that simultaneously computes the epicenters and the station corrections in an iterative process. VELEST code requires an initial velocity model, travel times for each earthquake-station pair, station coordinates and delay times.

To account for lateral variations in the shallow subsurface, station coordinates are included in the inversion. Velocity calculation procedures do not guarantee convergence to a best solution. The steps of minimum 1-D velocity model calculation will be given extensively in the following section.

4.3. Calculation Steps of the 1-D Minimum Velocity Model

1-D Minimum P-wave velocity model is calculated by four-step process. The steps of calculation of minimum 1-D model have been developed through the application of Equation 4.3 in many areas of both simple and complex crustal structure around the world (Kissling *et al.,* 1994).

4.3.1. Establishing the Priori 1-D Model(s)

All priori information regarding the area under study should be obtained (layer velocities and thicknesses) as previously mentioned above (Chapter 4.2). This information may include seismic reflection and refraction studies or a general crustal model. The media should be defined by several layers of increasing velocity with depth (Kissling *et al.*, 1994). Layer thicknesses should be 2-3 km in the upper crust and 4-5 km in the lower crust. To probe the dependence of the solution on the initial model one should try at least three different initial velocity models for any model geometry (layer thickness): one with extremly low crustal velocities, one with extremly high and one with intermediate crustal velocities (Velest User's Guide). After this step this model is called a “priori” 1-D velocity model.

4.3.2. Establishing the Geometry and the Velocity Intervals of Potential 1-D Model(s)

The best events with high quality P arrivals in the data set should be selected to cover the entire area. These events are relocated by VELEST using the appropriate damping values for each model parameter. This procedure is repeated for several times with updated (new) velocities, station delays and hypocentral parameters. In addition, adjacent layers with similar velocities can be combined during the inversion.

The procedure in this second step should also be applied for the combined layers. In most cases, low velocity layers should be avoided due to the instabilities they introduce to the problem.

Kissling *et al.,* (1994) suggest that shot or blast data (controlled-sources) should not be used in the inversion. Rather such data can be used to test the performance of the final minimum 1-D model. We can proceed to the next step if the following criteria are reached: the earthquake locations, station delays and velocity values do not vary considerably in subsequent runs, RMS values of all events indicate a considerable reduction, the calculated 1-D velocity model and the station corrections make geological sense.

If all these requirements are fulfilled the resulting model can be called the “updated a

priori 1-D model with corresponding station residuals" (Kissling *et al.,* 1994).

4.3.3. Relocation and Final Selection of Events

All events are relocated using the updated velocity model with HYPO71 (Lee and Lahr, 1975), HYPOCENTER (Lienert and Haskov, 1995) and VELEST in the single event mode, however there were no significant differences between two results.

4.3.4. Evaluation of Minimum 1-D Model

The step 2 is repeated with the new data set obtained from step 3 with the relevant damping parameters. This step is executed in order to find the best velocity model that minimizes the overall location errors for the fixed geometry. This step is repeated until the satisfaction requirements in step 2 are reached.

4.4. Calculation of 1-D Minimum Velocity Model for Isparta Angle and Surroundings

A total of 297 events with azimutal gap less than 180˚ and with at least 6 P-phases were selected from the initially located data set (total number of 875 events) for the (1-D) velocity inversion via VELEST algorithm. The selected events (blue circles) and their depth distribution (latitude and longitude depth cross-sections) are shown in Figure 4.1 along with the initial earthquake locations based on a certain data selection criteria mentioned above.

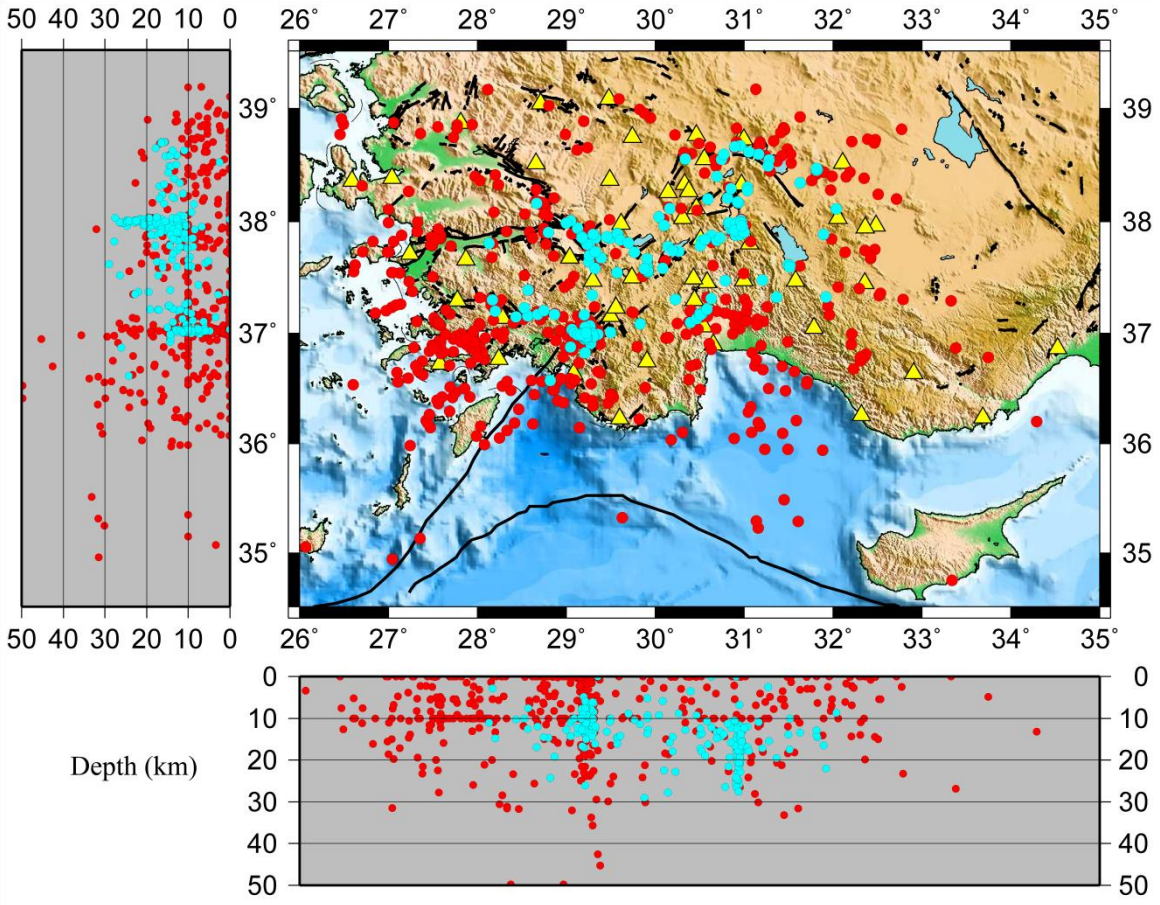

Figure 4.1. Events used for the 1-D P-wave velocity inversion (blue circles) with their depth distribution and the initial locations (red circles)

Azimuthal gap values vary between 51° and 180° (GAP ≤ 180°) with an average of 128° in the selected data set for the 1-D inversion. The average root mean square (RMS) value for the selected data set is 0.5 seconds and RMS values of the selected events vary between -1.0 and 1.0 seconds.

We used the 1-D velocity model (which is also used by KOERI to perform earthquake location procedure) as a starting point.

A total number of 297 well locatable events (with a total number of 3725 P phase readings) were used in the 1-D velocity inversion with two steps and ten iterations for each run. The media was defined by several layers of increasing velocity with depth as mentioned in the previous section (calculation steps). We used three different velocity

models to probe the difference on the initial model: one with extremely low, one with extremely high and one with intermediate crustal velocities (Figure 4.2).

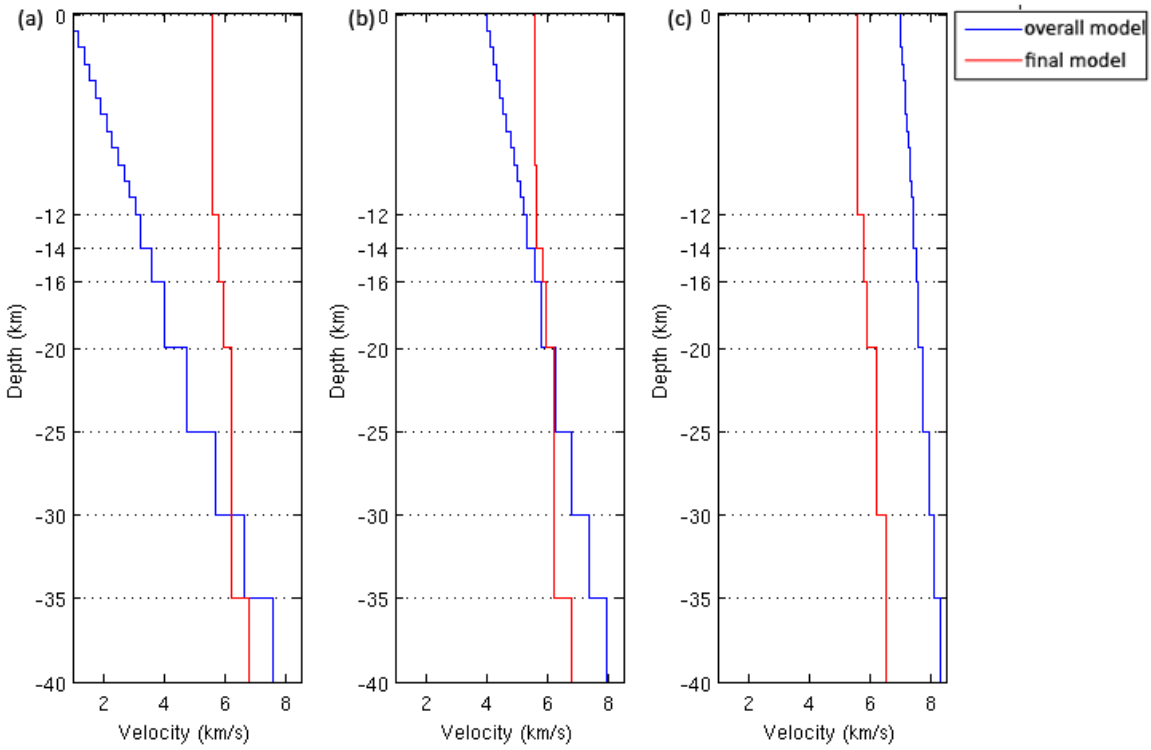

Figure 4.2. Inversion results for three trial P-wave velocity models (blue lines): (a) model with low P-wave velocities, (b) model with intermediate P-wave velocities, and (c) model with high P-wave velocities. Red lines denote the output P-wave velocity models

Depth range of the velocity models varies between 0-40 km due to the crustal structure and station elevations. Hypocenter locations, velocities and station delays are updated for each run. Adjacent layers with similar velocities were combined for each velocity inversion run. As seen in Figure 4.2, we observed a considerable convergence in velocity values for 0-35 km depth range which means that 0-35 km depth range is well resolved by the data. However, trial velocity models are not accurately constrained below 35 km depth due to the lack of seismicity below this depth.

A new velocity model depending on initial runs was contructed and resulting velocty model was kept after a new inversion run. In Figure 4.3, the overall output velocity model obtained from the three previous runs (solid blue line) is again inverted with the updated

inversion parameters and the relevant control parameters.

A mean model that is called “an updated priori 1-D model” was constructed by using three output models. Relocated data set was inverted with the updated velocity model and the station correcitons (Figure 4.3). As seen on Figure 4.3, we did not observe a significant change in velocities for a run with new constructed model. Resulting model after inverting newly constructed model is depicted with red solid line in the Figure 4.3.

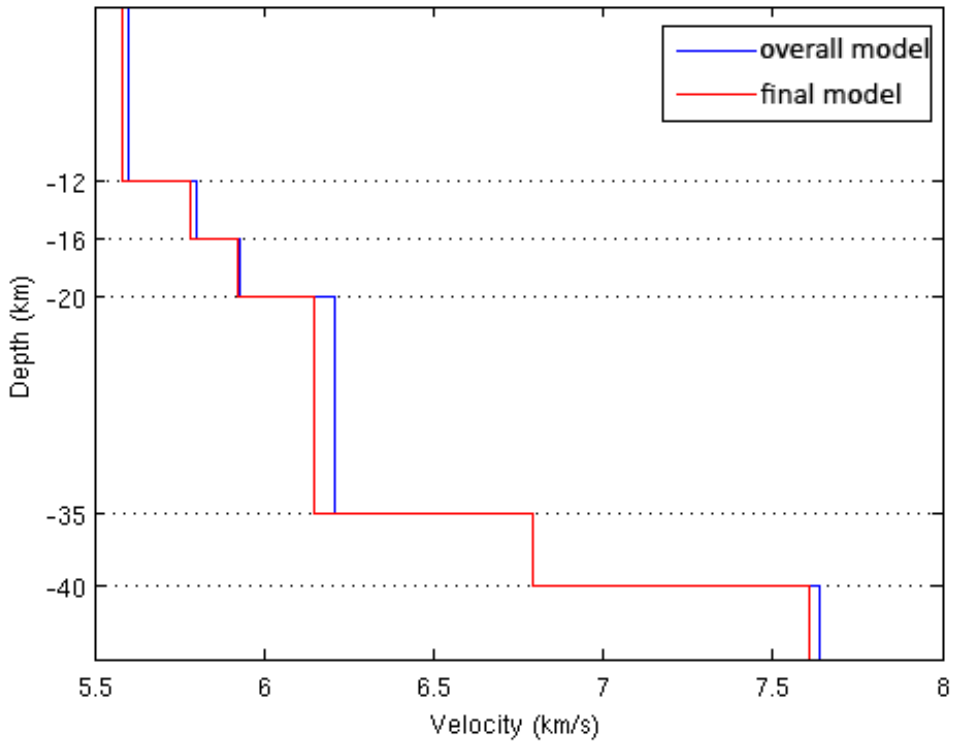

Figure 4.3. Inversion results for the resulting velocity model (blue line) from the previous inversion with three different trial velocity models. Red line represents the output velocity model

Two velocity models seemed to be well converged for the depth range between 0-35 km. We call this resulting velocity model “updated a priori 1-D velocity model” with the corresponding station residuals.

Furthermore, another velocity inversion was performed using the initial data set along with the updated station residuals from the previous inversions. All events were

relocated by VELEST in “single event” mode with the updated P wave velocity model (Figure 4.4). The final inversion did not also show a significant difference in subsequent runs and the output model looked to be consistent with the given updated input velocity model. Moreover, the RMS values and the data variance have considerably decreased as a result of the several iterations in the velocity inversion.

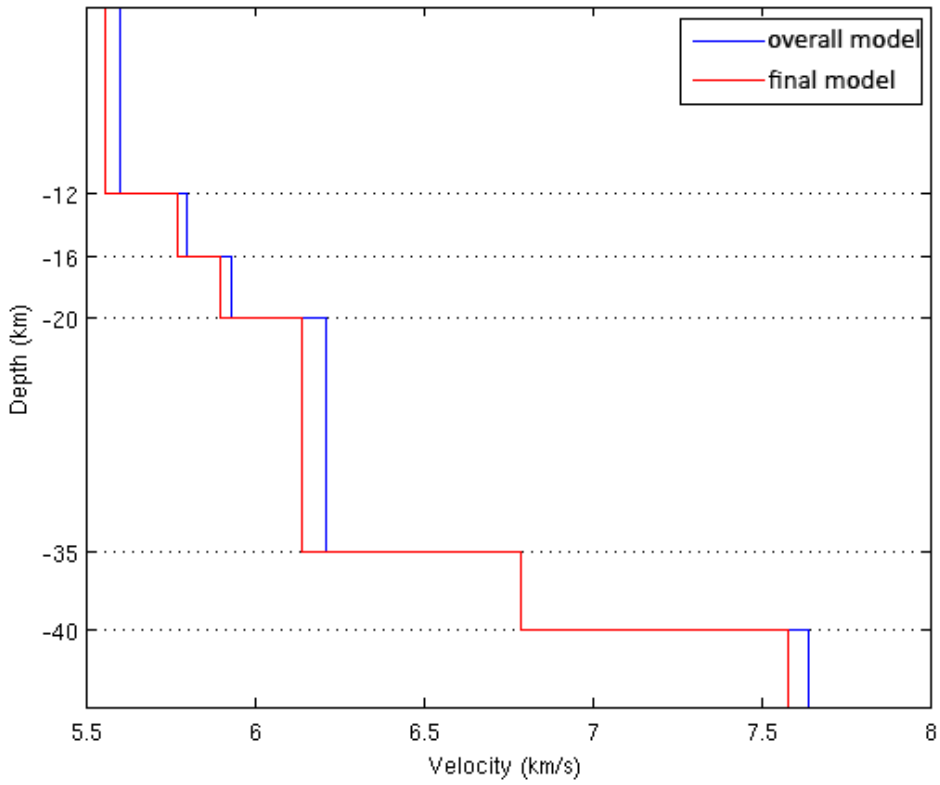

Figure 4.4. Inversion results of the relocated data set with the updated velocity model and the station corrections. Blue line represents the input model and the red line represents the output model

After two of trial and error inversions, final minimum 1-D velocity model for Isparta Angle and Surroundings was derived and shown in Figure 4.5.

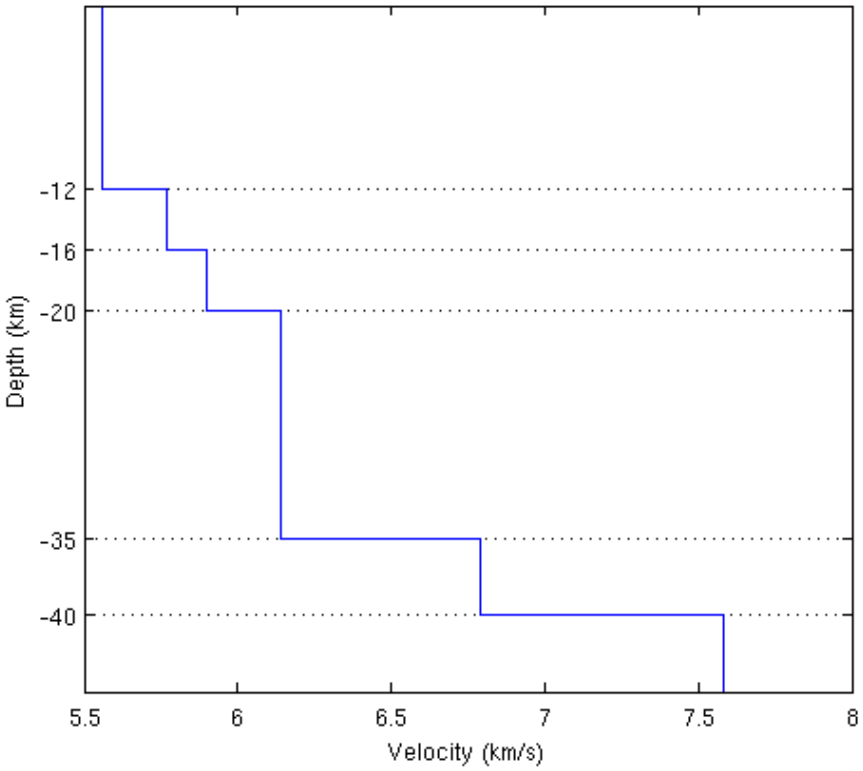

Figure 4.5. 1-D Minimum P-wave velocity model for Isparta Angle and surroundings obtained from the previous velocity inversions (blue line)

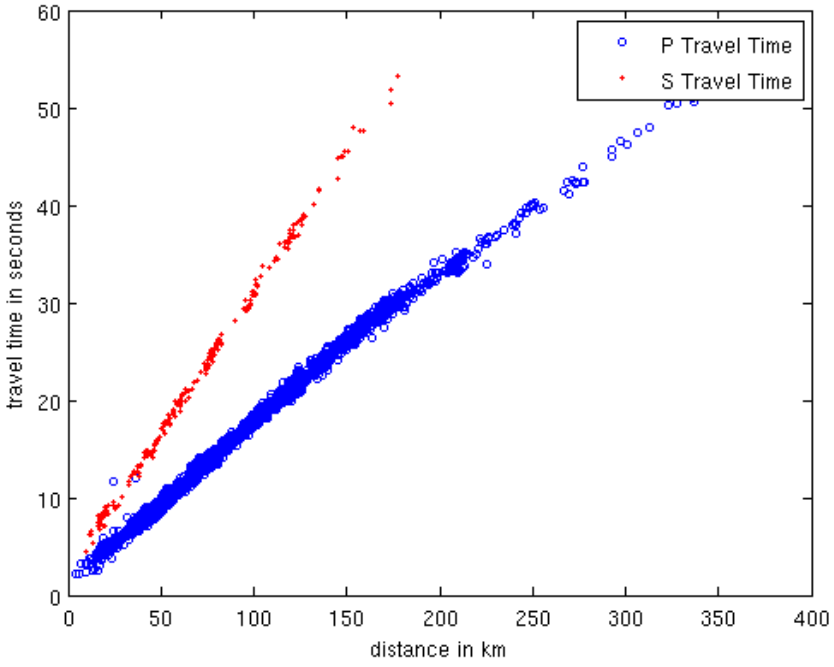

Figure 4.6. Travel time curves for P and S pickings

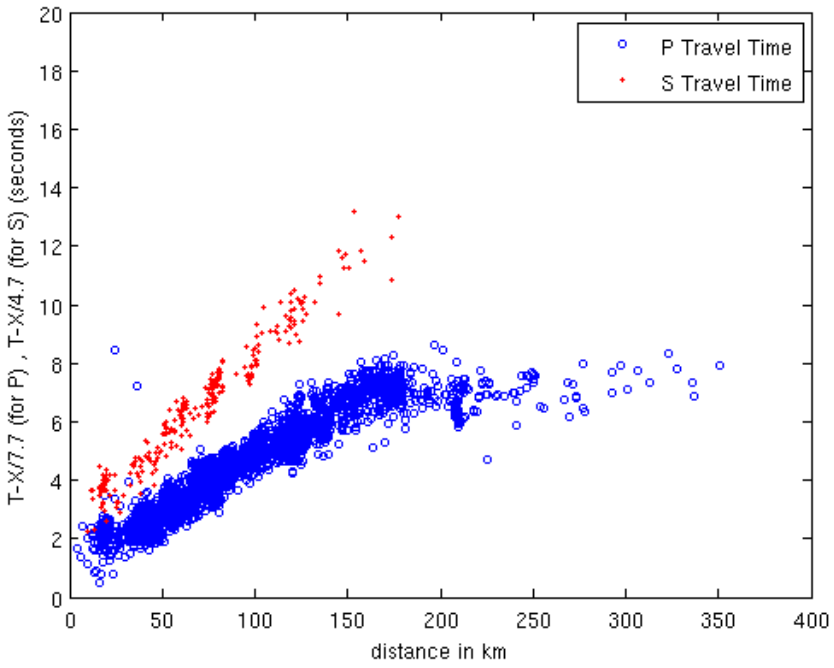

Figure 4.7. Travel time curves for P and S pickings (with reducing velocity)

Figure 4.6 illustrates the travel time curves for P and S pickings and the distances. Figure 4.7 also shows the travel time curves but with reducing velocity values. Reducing velocity values (7.7 km/s for P, 4.7 km/s for S) are used to clearly see Pn and Sn phases.

Compared to the initial 1-D velocity model, the minimum 1-D P wave velocity model led to a reduction in RMS and azimuthal gap values. The observed average RMS value has reduced from ~0.5 seconds to 0.39 seconds and the data variance has reduced to 0.25. After the velocity inversion and the relocation of initial data set with the minimum 1-D velocity model, average gap values decreased from 129° to 128°. An average Vp/Vs value of 1.80 was used to constrain the S-phases and the earthquake depths more accurately.

4.5. Stability Tests for the 1-D P-Wave Velocity Model

The stability of the 1-D minimum P wave velocity model is tested to assess the model quality. Every hypocenter is shifted 7 to 8 kilometers in each direction (x, y, z) with the actual value obtained from a random distribution. Shifting process was performed through a fixed velocity model (highly overdamped velocity values). Then, shifted

hypocenter values are inverted again to test if they get their initial values. The further results of the random and systematic event shifting tests are given in the following sub-sections.

4.5.1. Systematic Shifting Test

Final hypocenter locations were systematically shifted in three coordinates (red dots in Figure 4.8) with a constant shifting value of 9.5 km in latitude (north), 9.6 km in longitude (east) and 10 km for depth (downwards). The simultaneous inversion with 15 iterations was performed for a fixed velocity model (Figure 4.5) that allows the hypocenters float during the process. Both hypocentral and model parameters (with the station corrections) were inverted in every second iteration to avoid the hypocenter-velocity structure coupling.

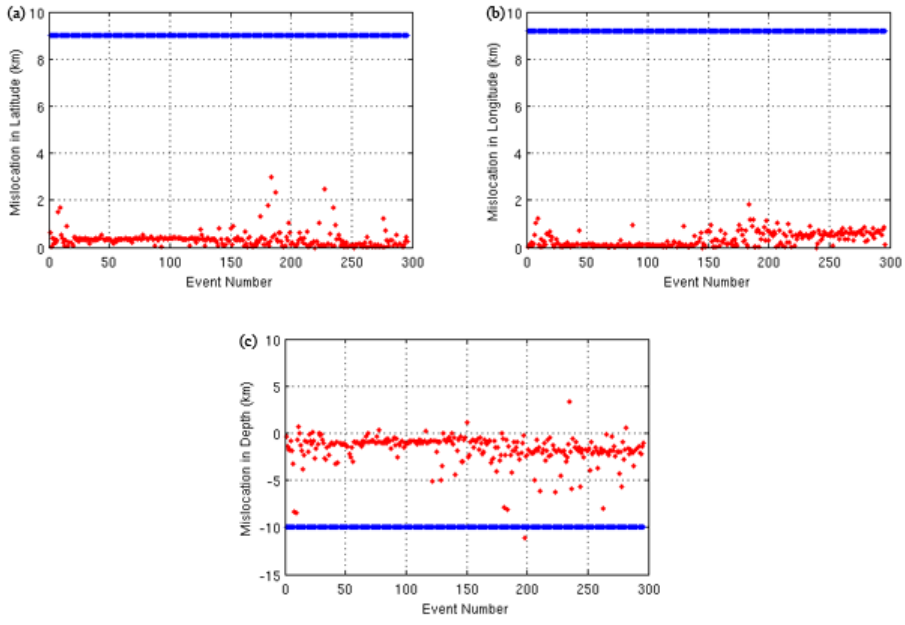

Figure 4.8. Inversion results after applying constant shifting values for the fixed velocity values. Blue dots denote the shifted hypocenters and the resulting hypocenters are indicated with red dots. (a) Latitude shift (km) (b) Longitude shift (km) (c) Depth shift (km)

Figure 4.8 indicates that the event mislocation in latitude and longitude is lower than 1 km with an average of 0.334 km in latitude and 0.326 km in longitude. These values state

that majority of the shifted hypocenters closely recovered to their original locations after the simultaneous inversion. On the other hand, event mislocation in depth is between 0 and 5 km for most of the shifted hypocenters with an average of 1.69 km (downwards). Higher mislocation values might be caused by the uncertainties in the depth calculation of initial hypocenters.

4.5.2. Random Shifting Test

Following the systematic shifting test, another stability test was performed by randomly perturbing the initial hypocenters 5-7 km in each direction. Latitude and longitude values are shifted to a certain positive value mentioned above, but the depth values are shifted both to positive and negative values. The simultaneous inversion with 15 iterations was performed for a fixed velocity model (Figure 4.5) that allows the hypocenters float during the process. Both hypocentral and model parameters (with the station corrections) were inverted in every second iteration as a basic procedure.

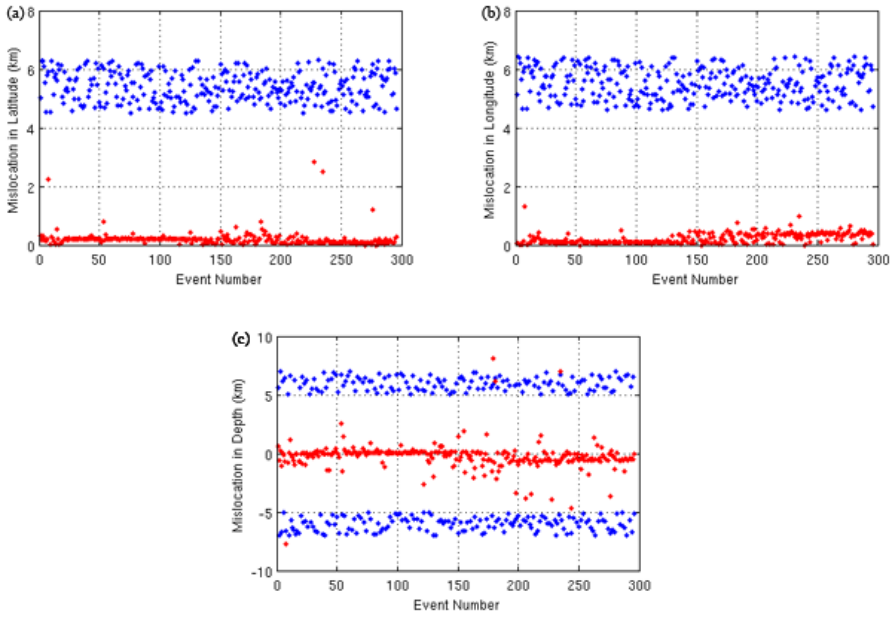

Figure 4.9. Inversion results after applying random shifting values for the underdamped velocity values. Blue dots denote shifted hypocenters and red dots denote resulting hypocenters. (a) Latitude shift (km) (b) Longitude shift (km) (c) Depth shift (km)

Figure 4.9 illustrates that, with a few exceptions, the majority of event mislocations

in latitude and longitude is lower than 1 km with an average of 0.321 km in latitude and 0.336 km in longitude. We have observed a slight increase in longitude mislocation and a decrease in latitude mislocation compared to the systematic shift. On the other hand, event mislocation in depth is between 0 and 5 km for most of the shifted hypocenters with an average of 2.50 km (2.5 km for upward and -2.5 km for downward).

Consequently, after the random and the systematic event shifting tests overall mislocation results looked to be consistent within each other suggesting that “1-D minimum P-wave velocity model” has the sufficient resolving power in terms of model stability.

5. THREE DIMENSIONAL (3-D) VELOCITY TOMOGRAPHY

LET is useful method to improve the estimates of the model parameters such as structure and hypocenters. Thurber (1993) indicates that LET has some advantages over teleseismic tomography, the potential for higher resolution imaging of the structure due to higher frequency content of local earthquakes, closer station spacing and the presence of sources within the model volume that generally allows for finer spatial sampling.

Compared to the controlled-source tomography, LET offers substantial excitation of both compressional and shear waves and their three-dimensional (3-D) spatial distribution. An important drawback, however, is the lack of independent knowledge of the exact event locations and origin times.

Thurber's (1983) method of iterative simultaneous inversion for three-dimensional velocity structure and hypocenter parameters using travel-time residuals from local earthquakes was employed. Key features of this method which allow the problem to be computationally feasible are parameter separation and approximate ray tracing.

After relocation of all events with the minimum 1-D P-model, a selection for a gap 180˚ and at least 6 P-readings yielded a data set of 297 events with 3725 P-readings, which were then used in the 3-D inversion. No inversion for S-velocities is undertaken in this study.

First of all, appropriate node-grid spacing for 3-D initial P-wave velocity model is determined through seismometer spacing. And then P-wave velocity damping factor were determined by employing trade-off curve tests which will be explained in detail in the following chapters. A series of 3-D P-wave velocity inversions were employed after determining node-grid spacing and P-wave velocity damping factor. And then, resolving capability of resulting 3-D P-wave velocity model was tested.

In the following sections, the basic theory of LET including the major aspects of the problem and the tomographic application for Isparta Angle and surroundings will be given.

5.1. Basic LET Theory

Travel time of a body wave (T) from an earthquake (i) to station (j) is expressed using ray theory (Thurber, 1993).

$$T_{ij} = \int_{source}^{receiver} u\mathrm{ds} \tag{5.1}$$

In Equation 5.1, u is slowness field and ds is an element of path length. However in practice, actual observed travel times are T_{ij}:

$$t_{ij} = \tau_i + T_{ij} \tag{5.2}$$

τ_i is earthquake origin time. In LET problem, eventhough known parameters are station coordinates and observed travel times, they have some uncertainities. Sources are distributed within the model volume (Thurber, 1993).

In this case observed travel times (t_{ij}^{obs}) are measured from network, calculated travel times (t_{ij}^{cal}) are determined from Equation (5.1) and Equation (5.2) using trial hypocenters, origin times and priori velocity model. The difference between observed and calculated travel times is called travel time residuals (Equation 5.3).

$$r_{ij} = t_{ij}^{obs} - t_{ij}^{cal} \tag{5.3}$$

The residuals can be related to desired perturbations to the hypocentral and velocity parameters by a linear approximation indicated in Equation 5.4. $\partial T_{ij}/\partial x_k$ indicates the hypocentral derivatives, $\Delta\tau_i$ represents the origin time perturbations, u represents the slowness.

$$r_{ij} = \sum_{k=1}^{3} \frac{\partial T_{ij}}{\partial x_k} \Delta x_k + \Delta\tau_i + \int_{source}^{receiver} \delta u\mathrm{ds} \tag{5.4}$$

Following Thurber (1986) the hypocenter partial derivatives $\partial T_{ij}/\partial x_k$ are proportional to the components of the ray vector times the seismic slowness at the source point.

$$\frac{\partial T_{ij}}{\partial x_k} = -\frac{1}{V}\left(\frac{dx_k}{ds}\right)_{source} \tag{5.5}$$

If any finite parametrization is adapted to Equation 5.4, the resulting Equation will be the following.

$$r_{ij} = \sum_{k=1}^{3} \frac{\partial T_{ij}}{\partial x_k} \Delta x_k + \Delta T_i + \sum_{i=1}^{L} \frac{\partial T_{ij}}{\partial m_i} \Delta m_i \tag{5.6}$$

In this case m_i represents the L parameters of the velocity model.

Virtually all LET methods begin with Equation 5.4 and Equation 5.6. However they may differ to some extent based on some aspects such as, the scheme for the representation of the velocity structure, the treatment of the hypocenter-velocity structure coupling and the assessment of solution quality. These aspects will be covered in the following sections.

The ray theoretical approach taken has its limitations. The method makes use of first arrival times of seismic waves. It is implicitly assumed that these observed waves are direct arrival waves. As seismic energy propagates through some finite volume surrounding a "ray", not along an infinitesimal line, finite-frequency diffracted arrivals may not modelled by ray theory.

5.2. Representation of Velocity Structure

There are a wide variety of ways to represent velocity structure of a region in LET problems and they are all only approximations to the real 3-D velocity structure. Earth's crust and upper mantle has heterogeneous structure including faults, discontinuities, layering, intrusions and also anisotropy. Following Thurber (1993) in LET problems, solving capability of Earth's heterogeneous structure is depends on many factors such as density of ray sampling and minimum wavelength of recorded seismic wave energy.

Figure 5.1 depicts the constant-velocity block approach of Aki and Lee (1976) that treats Earth as a set of boxes within each of which seismic velocity is constant.

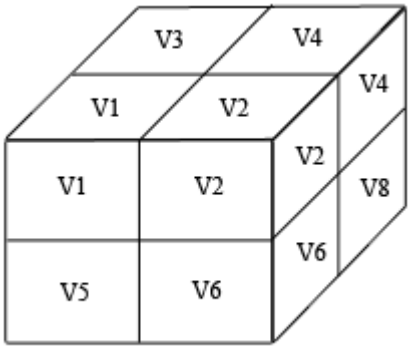

Figure 5.1. The constant-velocity block approach of Aki and Lee (1976) (After Thurber, 1993)

Although this approach has the advantage of simplicity, it is clearly lacking the ability of determine heterogeneous structure faithfully. However this limitation is slightly overcame by allowing gradual and rapid velocity changes from block to block. Unfortunately the vast number of blocks again results in problem being under-determined and some computational difficulties.

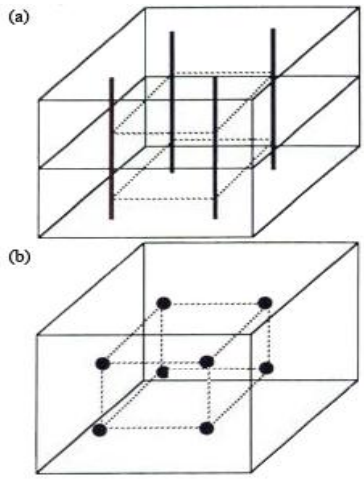

Figure 5.2. Laterally varying layers (a) and a grid of nodes (b). Dashed lines indicate the spatial form of interpolation (After Thurber, 1993)

Figure 5.2 illustrates that variations on discrete block parametrization include

laterally varying layers (Hawley *et al.,* 1981) and a 3-D grid of nodes (Thurber, 1983). The model is divided into layers in which velocity is constant in the vertical direction; however, velocity is obtained by interpolation among vertical nodal lines in the horizontal directions (Hawley *et al.,* 1981). Thurber (1983) used a 3-D grid approach that velocity varies continuously in all directions (Figure 5.2b). Another approach is to consider each set of four neighboring nodes as defining the vertices of thetrahedron (Lin and Roecker, 1990). Snell's law is used at tetrahedral boundries. This approach can use an analytic ray-tracing procedure, as ray-paths are circular arc segments in a medium with constant velocity gradient.

There are also other choices for representing Earth structure in LET. Each LET application is unique, accounting in part of the diversity of methods developed to represent structure. An appropriate velocity structure representation should be made based on the data set that will be analyzed.

5.3. Ray-Path and Travel Time Calculation

As travel time of a seismic wave along a path is needed to calculate arrival time residual and raypath of this wave is needed to compute hypocentral parameters, these parameters should be solved in order to use LET method. There are many ways to determine these parameters and the method chosen for representing Earth structure generally tends to define the most appropriate way of solving these parameters, or vice versa. Some limited numerical testing can be done to eliminate errors that may occur as a result of the errors in travel time or raypath itself.

Ray-tracing is a two-point boundry value problem (BVP); boundries are source and receiver, and the propogation path and time must be determined. There are some methods to solve this boundry value problem. Shooting methods solve the two-point BVP by iteratively solving an initial value problem (IVP) with one fixed end-point, however bending methods solve BVP directly by keeping two end-points fixed (Figure 5.3).

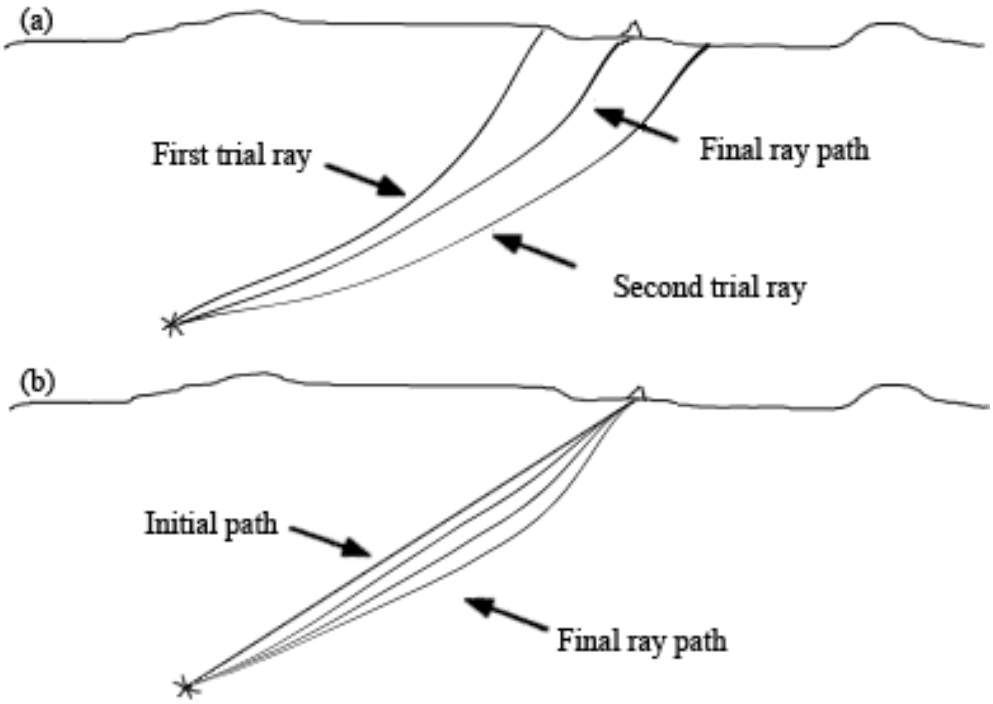

Figure 5.3. Two basic approaches of ray tracing: (a) shooting method, (b) bending method (After Thurber, 1993)

As seen on Figure 5.3a, for shooting method, the trajectory of the initial ray at the source is perturbed until the receiver is reached. For bending, an initial path (not a ray path) connecting the two-end points perturbed until a ray-path is reached (Figure 5.3b). As mentioned above the method to represent velocity structure tends to define the method to determine ray-path and travel-time calculation. However, modern technology makes it easy to use powerful computers, so large-scale problems may become easy to solve.

5.4. Hypocenter-Velocity Structure Coupling

In general, LET method is known as a method that fixes the hypocentral parameters during the inversion process, however, in simultaneous inversion, hypocentral parameters are coupled with velocity parameters. Therefore, one of the most important sections of the study is the proper treatment of mathematical coupling between hypocentral and velocity parameters. If the direct treatment over these parameters is required, an immediate concern is the growth of the matrix size represented by the Equation 5.6.

Fortunately, a technique for taking the advantage of the sparse character of this matrix is available. The complete system of inversion equations can be written in the (discrete) form:

$$r = H\Delta h + M\Delta m \tag{5.7}$$

where r is the residual factor, H and Δh are the matrix and the vector of hypocenter parameter partial derivatives and perturbations, M and Δm are the matrix and vector of velocity parameter partial derivatives and perturbations, respectively. In geologically complex regions, ignoring the hypocenter-velocity structure coupling; that is, the term $H\Delta h$ in Equation (5.7) will inevitably result in systematic bias in the velocity model that will lead to hypocenter mislocation.

Furthermore, parameter separation was used by Pavlis and Booker (1980) as the practical technique to treat this coupling implicitly. This method is effective when the estimated hypocenters are linearly close to their true locations. In other studies, Thurber (1983) declared significant improvement in the model fidelity when the hypocenter-velocity structure coupling was included in the inversion equations.

5.5. The Inversion Method and Model Parametrization

One of the nagging questions in LET is to handle non-linearity of the problem. There are also other issues like high level heterogeneity of the crustal structure and gradual size of the matrix represented by the Equation 5.7. As mentioned above modern technology overcomes the issue of the gradual size of the matrix and high level of heterogeneity may be overcome by adopting an iterative approach through LET problem. These equations can be solved via Singular Value Decomposition (SVD) approach.

Equation 5.7 can be rewritten in matrix notation:

$$G\Delta m \cong \Delta d \tag{5.8}$$

In Equation 5.8, G represents the partial derivatives of model and hypocentral

parameters, Δm represents the model adjustments, Δd represents the difference between observed and calculated travel-time (residuals). There is a non-uniform ray sampling and distribution; therefore a perfect fit will never be satisfied. In this case the damping factors are initiated to overcome very small or zero eigen values.

After a proper rewrite of Equation 5.8 by adding the damping factor:

$$\Delta m \cong [G^T G + \lambda^2 I]^{-1} G^T \Delta d \tag{5.9}$$

I is the unity matrix and λ is the damping factor.

In this study SIMULPS14 software package that was originally developed by Thurber (1983, 1993) and improved by Eberhart-Philips (1986, 1993) was used to employ LET problem. This software package uses damped-least-squares and parameter separation technique (Pavlis and Booker, 1980) in order to solve LET problem. Parameter separation technique splits partial derivatives of model and hypocentral parameters (G) into hypocentral partial derivatives (H) and partial derivatives of model parameters (V). Equation 5.10 is the partial derivatives of model parameters after separation approach.

$$\Delta V \approx (V^T V + \lambda^2 I)^{-1} V^T \Delta d \tag{5.10}$$

The solution is strongly affected by the damping factor that depends on source-receiver geometry. In this study the damping value is selected by trade-off curve tests (Eberhart-Philips, 1986).

Another important nagging question in LET problems is model parametrization because it affects the solution and solution quality of the results. In terms of solution quality, coarse grid spacing yields large resolution estimates, whereas fine grid spacing yields low-resolution estimates.

P-wave velocity (Vp) and Vp/Vs values are determined at node-grid points (Figure 5.4) with variable spacing.

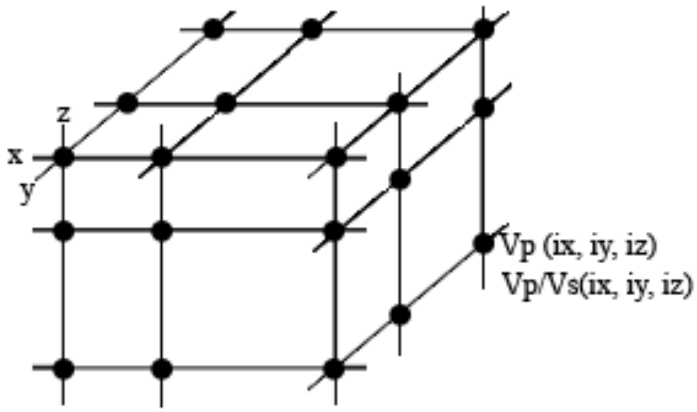

Figure 5.4. Node-grid geometry in SIMULPS14 (After Thurber, 1993)

Depending on the ray geometry, node-grid points can be either fixed by a threshold value for the minimum number of rays passing through a node-grid point.

5.6. Solution Quality of 3-D Inversion Process

Solution quality of 3-D inversion results depends on several measures such as data variance (misfit), resolution estimates and model covariance. Data variance is a measure of disagreement between the observed and predicted data. In case of obtaining the solution to the problem $G\Delta m \cong \Delta d$, an inverse G^{-1} is computed. The matrices of model resolution R and model covariance $C_m$can be calculated by the following equations:

$$R = G^{-1}G \tag{5.11}$$

$$C_m = (G^{-1})^T C_d G^{-1} \tag{5.12}$$

where C_d is the data covariance matrix (Menke, 1989). C contains the estimated variance of individual parameters and the covariation between pairs of parameters.

In addition to misfit and resolution estimates, several stability tests could indicate measure of quality to the solutions.

6. 3-D TOMOGRAPHIC INVERSION FOR ISPARTA ANGLE AND SURROUNDINGS

Three-dimensional tomographic inversion for Isparta Angle and surroundings was performed via SIMULPS14 software. SIMULPS14 software requires an input model that was constructed using 1-D minimum P-wave velocity model that was obtained from 1-D tomographic inversions. The earthquake data that was obtained from 1-D tomographic inversion was used as input to SIMULPS14. In the following sections, detailed information about input model generation, data selecting, solution capability of the data and selecting of P-wave velocity damping factor will be given.

6.1. Data Selection

The earthquake data and station correction parameters from 1-D tomographic inversion were used in 3-D tomographic approach for IA and surroundings. Figure 6.1 demonstrates the data set for the region, encompassing 297 earthquakes and 3725 P-wave observations in the period July 2006-June 2008. Data selection criteria were same as the previously performed one-dimensional velocity inversion.

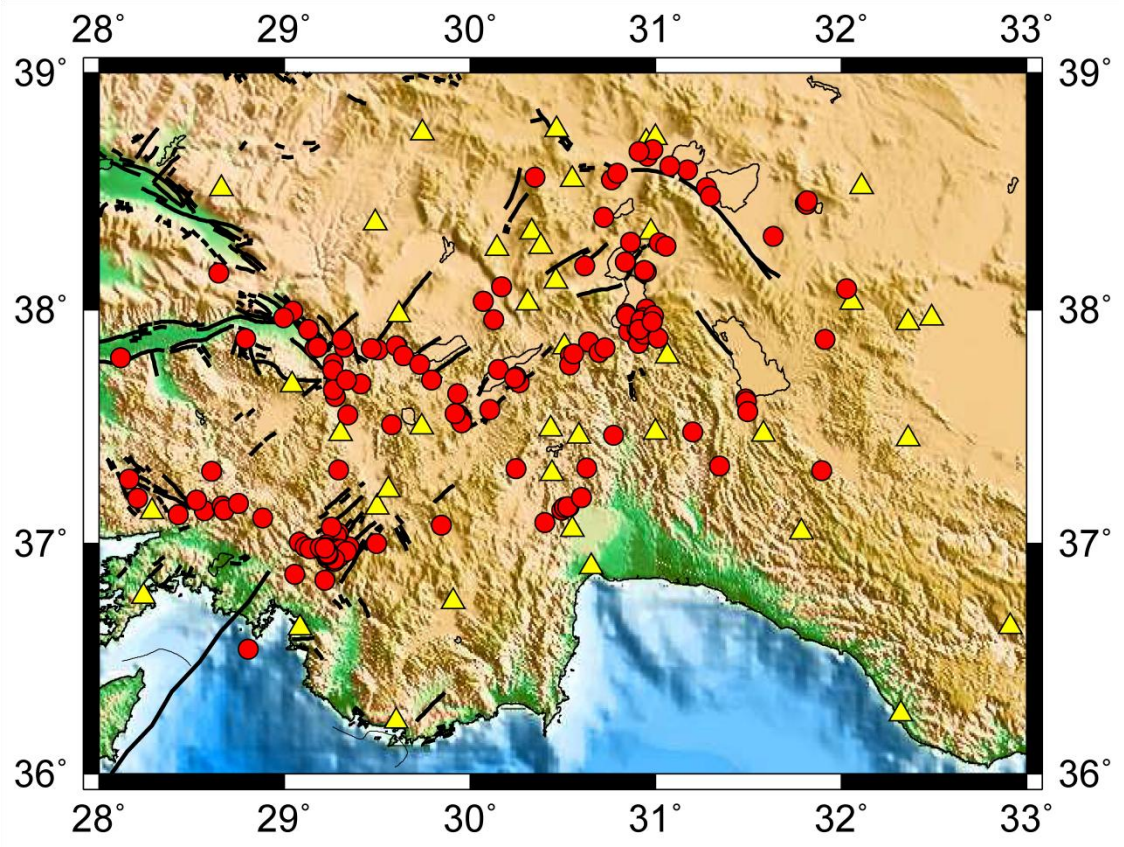

Figure 6.1. Selected event locations for the tomographic inversion. Yellow triangles represent the stations, red circles represent the events

6.2. Velocity Model Parametrization

As 3-D tomographic inversion requires a quality initial velocity model, the minimum 1-D P-wave velocity model is one of the most important parameter of this study. The model parametrization theory was explained in detail in Chapter 5.5.

Considering the station spacing and ray distribution of the data, a horizontal grid with 30x30 km node spacing was chosen for the 3-D inversion. Although, considering only the station spacing, 30x30 km and 25x25 km node spacing could be selected, ray distribution was not properly obtained for 25x25 km node spacing. Vertical grid spacing was taken from the minimum 1-D P-wave velocity model (Table 6.1).

Table 6.1. 1-D Minimum P-wave Velocity Model

Depth range (km)	**Velocity (km/s)**
0-12	5.56
12-16	5.77
16-20	5.90
20-35	6.14
35-40	6.79
40-	7.58

6.3. Control Parameters

One of the most important control parameters in LET is damping factor that is applied to velocity values because damping affects both results and resolution estimates. High damping values yield low model perturbations and low resolution estimates, whereas low damping yields high model perturbations and high resolution estimates.

Damping depends mainly on model parametrization on the average observational error (Kissling *et al.,* 2001). It can be determined by analysing trade-off curves between model variance and data variance for single-iteration inversion run in SIMULPS14 (Eberhart-Philips, 1986). In trade-off curve test, appropriate damping values show a significant decrease in data variance without a strong increase in model variance.

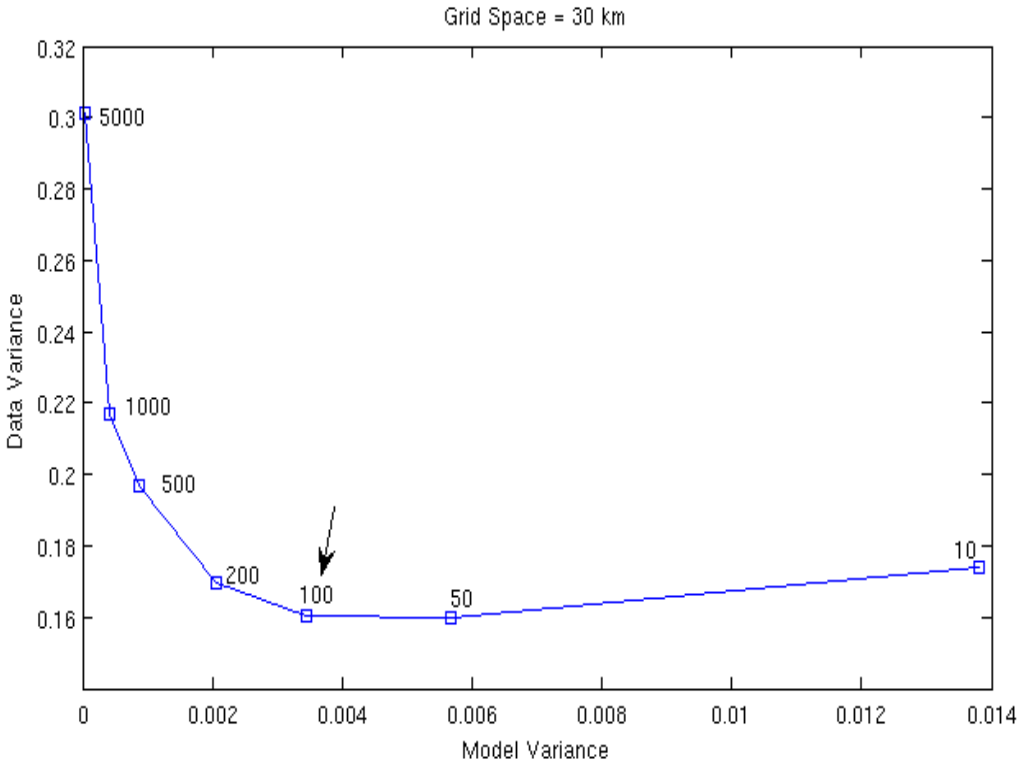

Figure 6.2. Trade-off curve test results

Figure 6.2 reveals that trade-off curve test indicated that the damping value that gives a significant decrease in data variance without a strong increase in model variance is 100 for this study

6.4. Resolving Capability

6.4.1. Resolution Parameters of Real Data

Resolution tests should be made in order to assess the reliability and quality of the results obtained. These resolution tests are hitcount (KHIT), resolution diagonal elements (RDE) and derivative weighted sum (DWS).

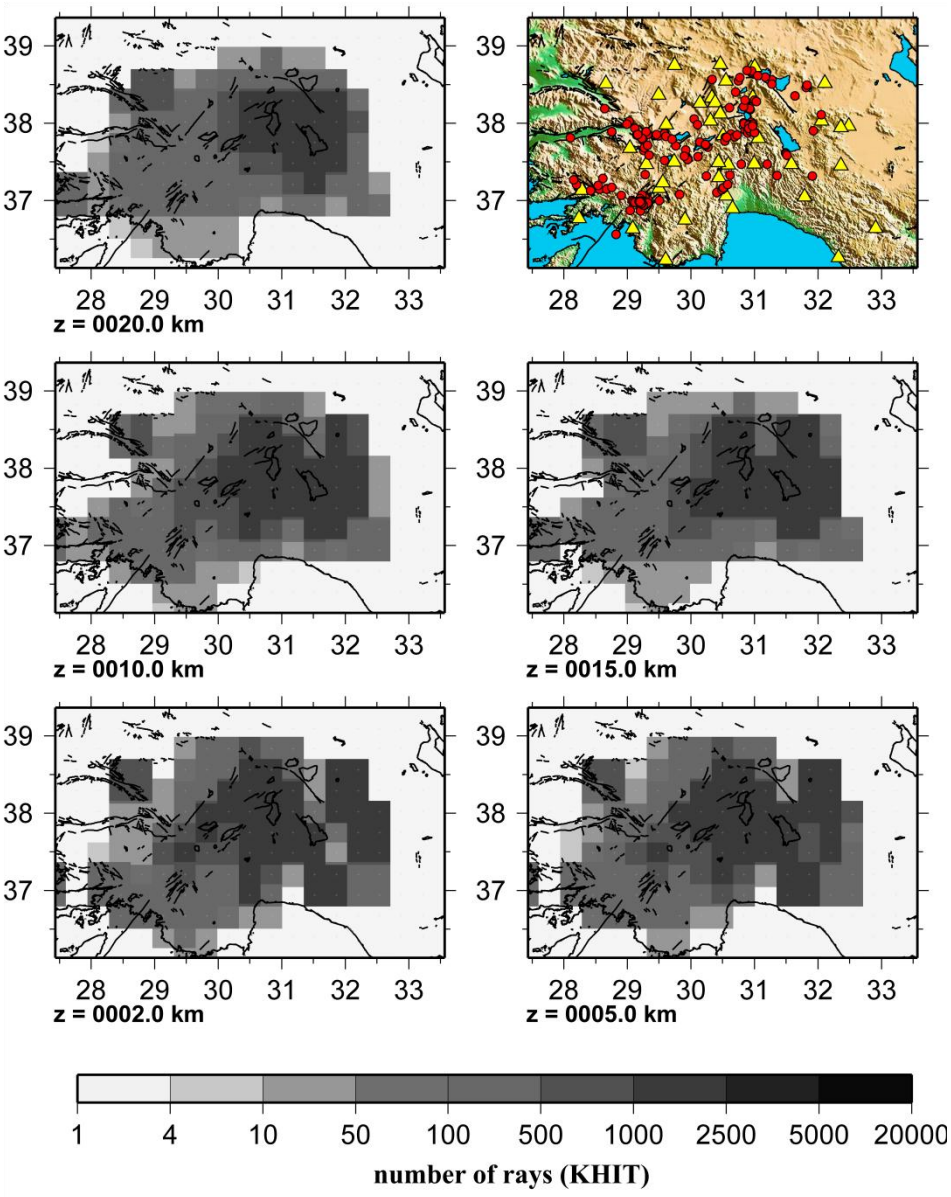

Figure 6.3. Horizontal depth sections of KHIT for the final Vp model. Events are shown by red circles, stations are shown by yellow triangles and small crosses denote grid nodes

KHIT denotes the number of rays that contribute to the solution at one node; the DWS indicates the relative ray density in the volume of influence of a model node. In this study, we define the solution as reliable if the model parameter belongs to an area that is well illuminated, as measured by the DWS (>800), and RDEs (>0.2).

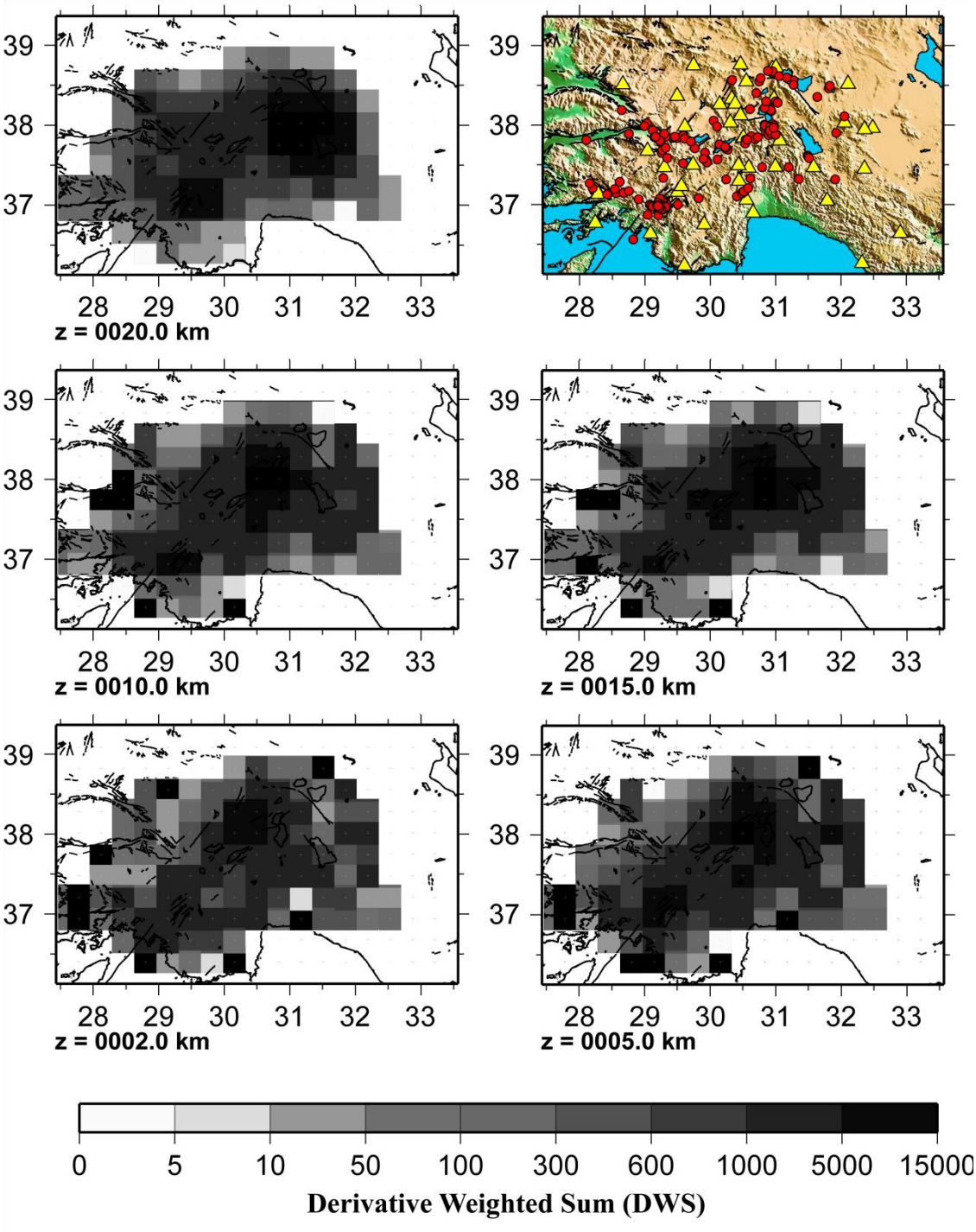

Figure 6.4. Horizontal depth sections of DWS for the final Vp model. Events are shown by red circles, stations are shown by yellow triangles and small crosses denote grid nodes

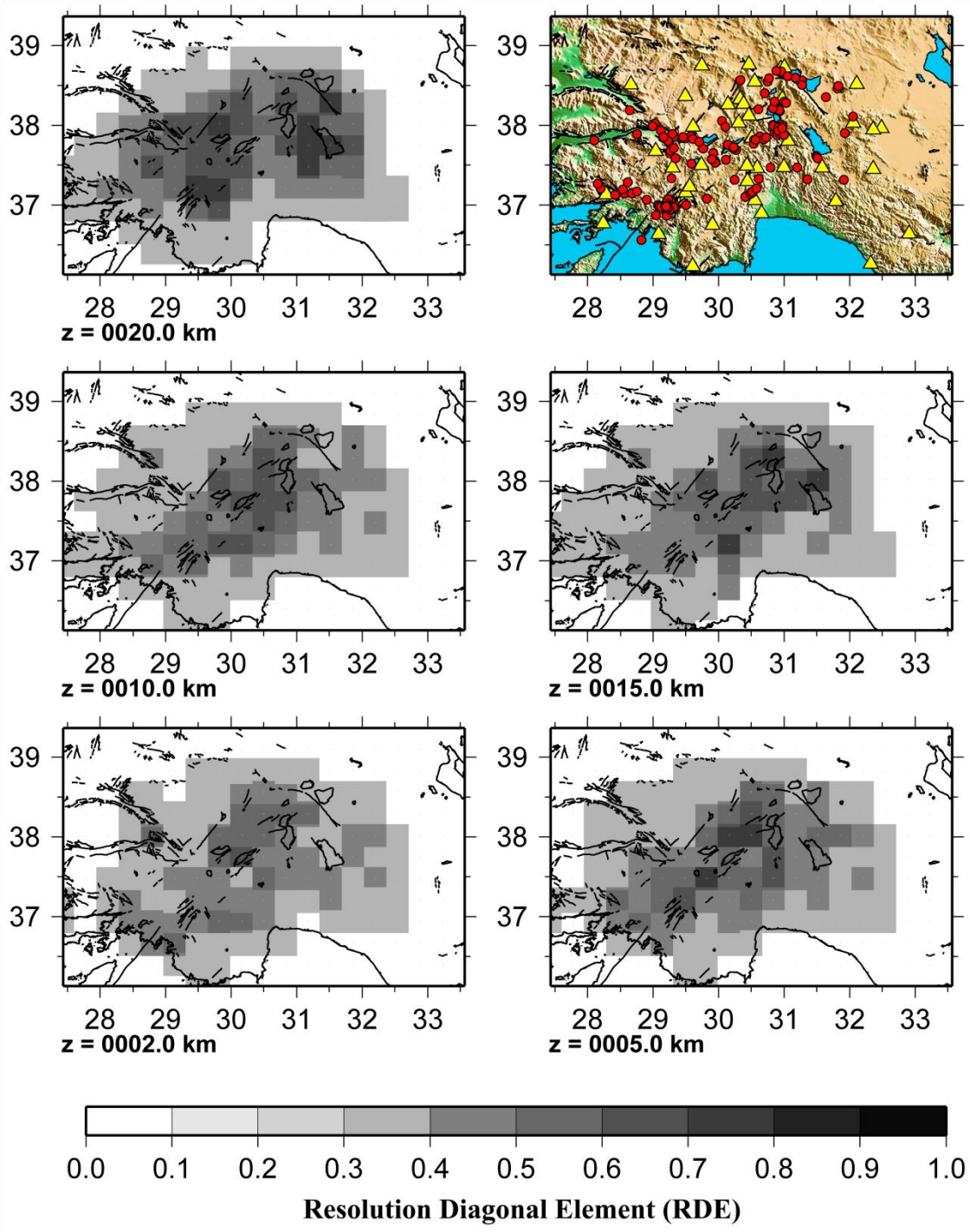

Figure 6.5. Horizontal depth sections of RDEs for the final Vp model. Red circles and yellow triangles represent the events and stations, respectively. Small crosses denote the grid nodes

As seen on Figure 6.3, number of rays (KHIT) from 2 km to 20 km depth is displayed respectively; this schema depicts that number of rays per node point more than 500, so the region is well illuminated. Figure 6.4 displays the derivative weighted sum

(DWS) for the real data and 3-D P-wave velocity model for this study. As seen on the figure DWS for this study is above 800 which means that the reliability of the study is high for the region of interest. The regions in the depth sections that are well illuminated are the same for the DWS and KHIT tests.

In Figure 6.3 and Figure 6.4, the KHIT and DWS perturbations for the different depth sections do not differ significantly, so we can say that the depth sections from 2-20 km are well illuminated in this study. The depth sections that were illuminated well has a minimum 0.3 resolution diagonal element (RDE) in general (Figure 6.5). This value is a significant indicator for the resolution capability of the model and data over the region of study. The RDEs also show the amount of independence in the solution for one model parameter. If the RDE is larger for one model parameter, the solution is more independent for this parameter. A more detailed discussion on resolution estimates is given in Toomey and Foulger (1989).

In this study, the resolution test parameters are poor relatively, so below 20 km is not displayed in these tests. RDE values is supposed to be “1” for identical case, however this value is not satisfied in these tests. These resolution tests give no information alone for the reliability of the resulting model and data.

6.4.2. Synthetic Data Test

As the resolution tests such as DWS, RDE and KHIT tests provide information related to resolve capability of the resulting 3-D P-wave velocity model and data for the region, synthetic data set also gives information about solution quality, model parametrization and damping factor assessment.

In synthetic data test, as first step; a synthetic data set is constructed by using a synthetic velocity model, as second step; data set is inverted with 3-D P-wave velocity model and synthetic data set. The perturbation between the synthetic model – 3-D resulting velocity model and synthetic model – output model of second step are compared. In identical case, two of the perturbations should be same; however this condition is never satisfied. The perturbation conformity for regions in the depth sections is proportional to

the resolving capability of the model over the region. Figure 6.6 depicts the synthetic input velocity model for the step 1 and the resulting output velocity from inversion of synthetic earthquake data obtained from step 1 and resulting P-wave velocity model of the study.

The synthetic 3-D P-wave velocity model was constructed by using initial 3-D P-wave velocity model. Two velocity values at grid node points were increased by ten (10) per cent, and velocity values at the following two grid-node points were decreased by ten (10) per cent. This process was initiated for whole velocity model in order.

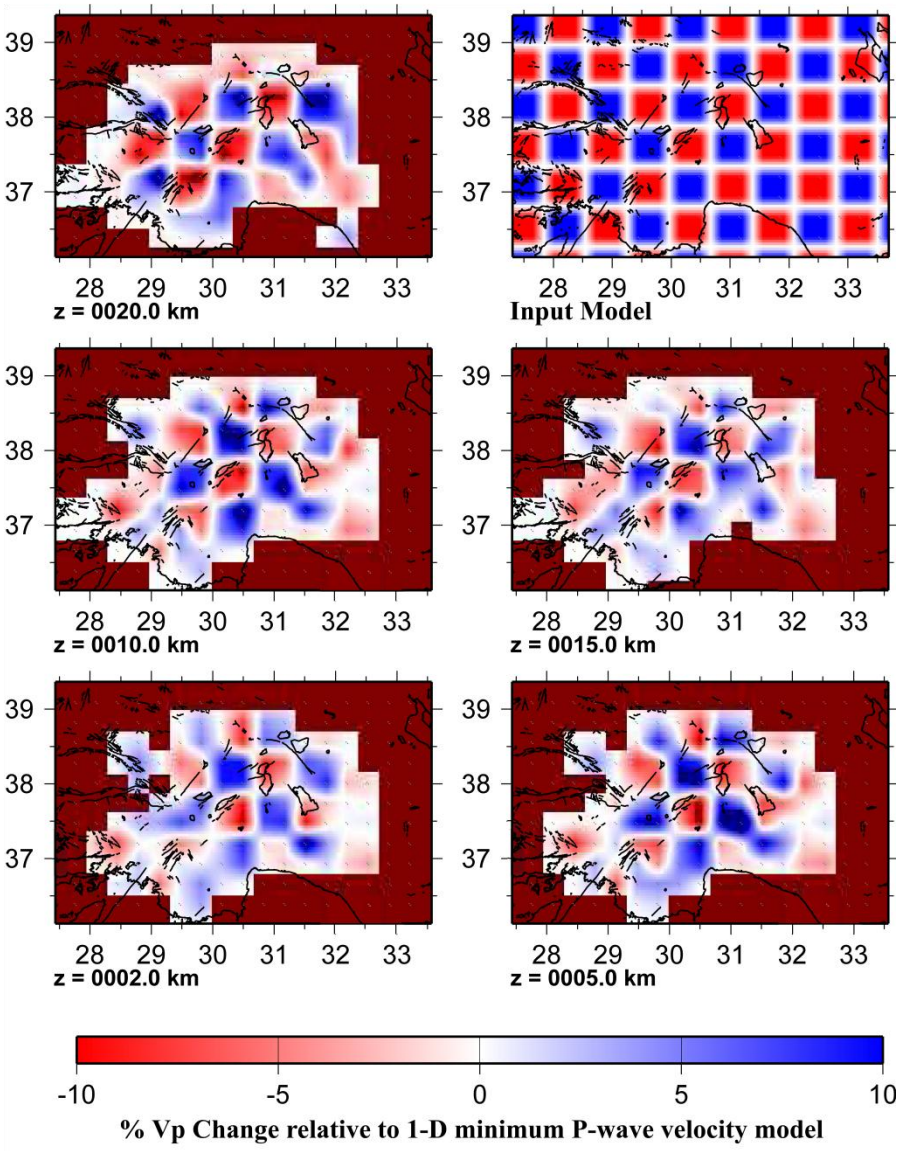

Figure 6.6. Synthetic model and horizontal depth sections for resulting P-wave velocity model perturbations from the initial 3-D P-wave velocity model for 2-20 km respectively after synthetic test

To perform a checkerboard test, positive and negative velocity anomalies of ±10 per cent were assigned to all the 3-D grid nodes as in input model (Figure 6.6). Synthetic arrival times are calculated for this input checkerboard model. Numbers of stations, events, and ray paths in the synthetic data are the same as those in the real data. The inverted image of the checkerboard suggests where the resolution is good and where it is poor. It is clear that the P-wave veloctity is well recovered down to 20 km depth. In general, stability of the model is relatively high for the center of the depth sections. Masked regions in depth sections denote the regions that are not hit by any ray. A synthetic model that has a denser grid space is generated (Figure 6.7).

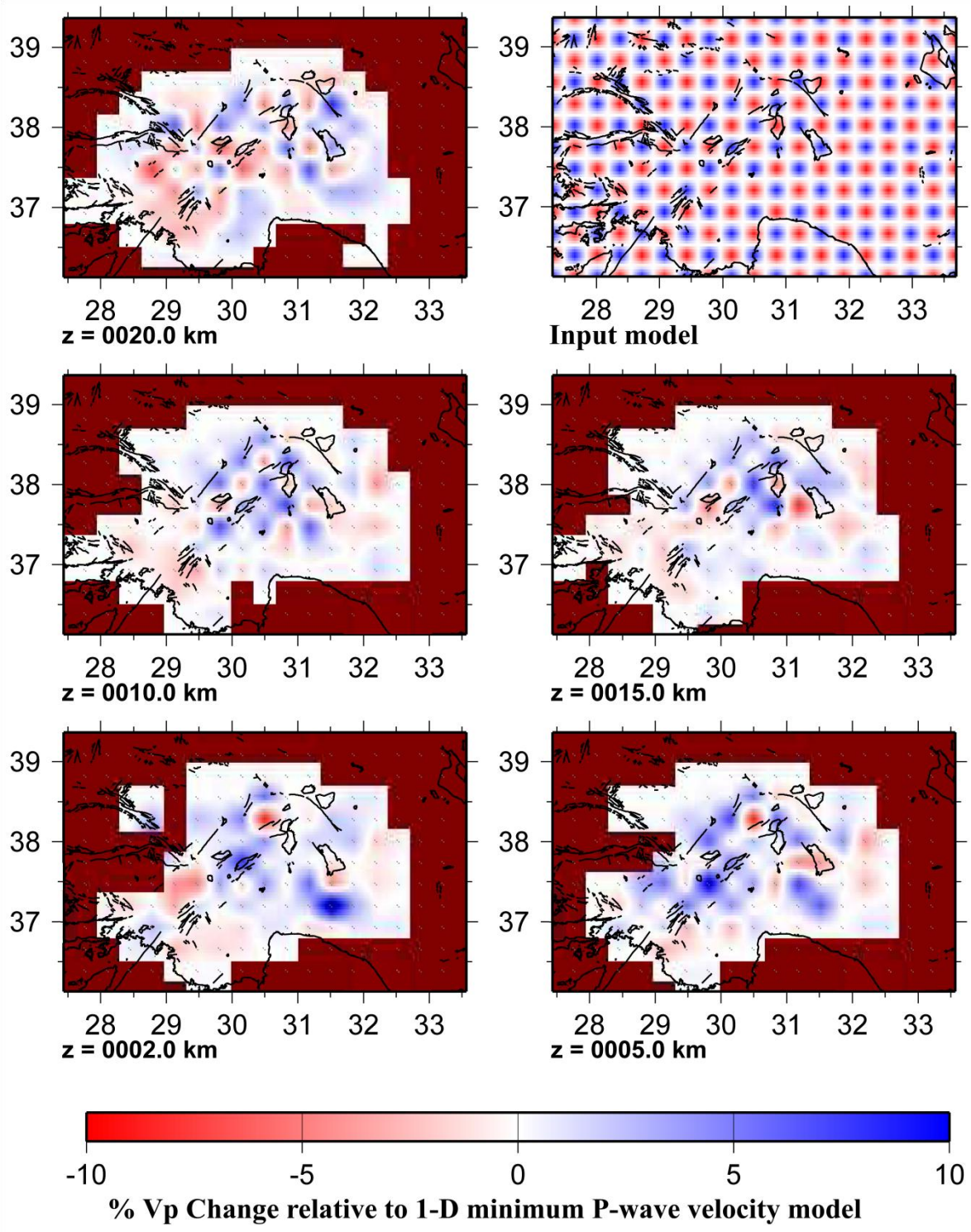

Figure 6.7. Synthetic model and horizontal depth sections for resulting P-wave velocity model perturbations from the initial 3-D P-wave velocity model for 2-20 km respectively after synthetic test

Figure 6.7 depicts the synthetic 3-D P-wave velocity model that has denser node-grid spacing than the former one has. As mentioned before, the similarity between synthetic model and output model of the test determine the resolve capability of the resulting 3-D P-wave velocity model over for the region.

It is clearly seen that the similarity of velocity perturbations between synthetic model and resulting model of this test increases for the depth sections from 2 km to 20 km. The regions, especially central part of the region in the 20 km depth section is resolved successfully. Regarding with the latter synthetic data test, it can be said that 20 km depth section is perfectly solved by the resulting 3-D P-wave velocity model.

6.5. Results of 3-D Tomographic Inversions

As we represented input model and damping factor of the 3-D tomographic inversion study, a two step and five iteration tomographic inversion via SIMULPS14 software was employed. Improved earthquake locations are shown in Figure 6.8.

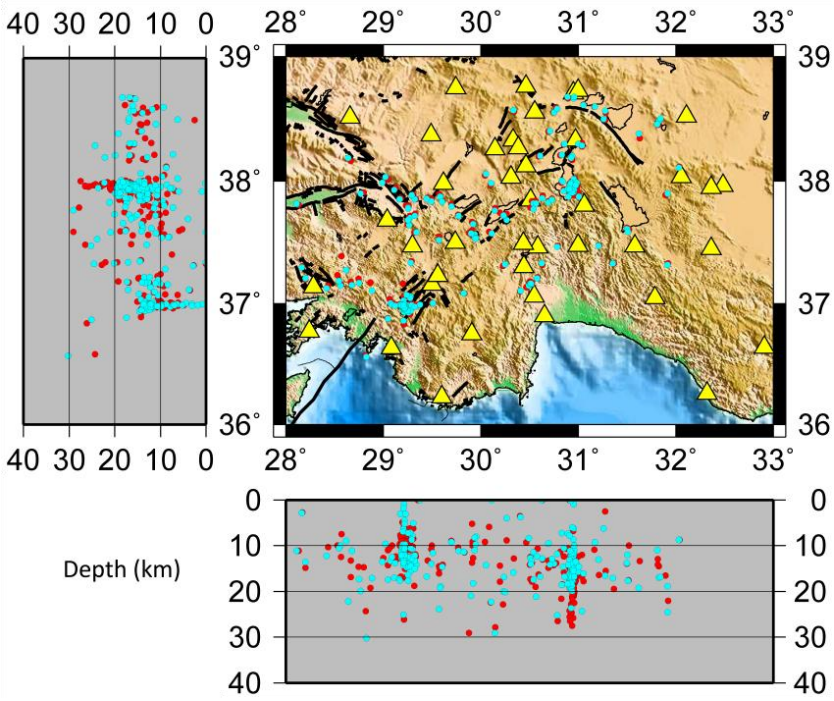

Figure 6.8. Improved earthquake locations. Red circles indicate initial earthquake locations, blue circles denote improved earthquake locations and yellow triangles mark the stations

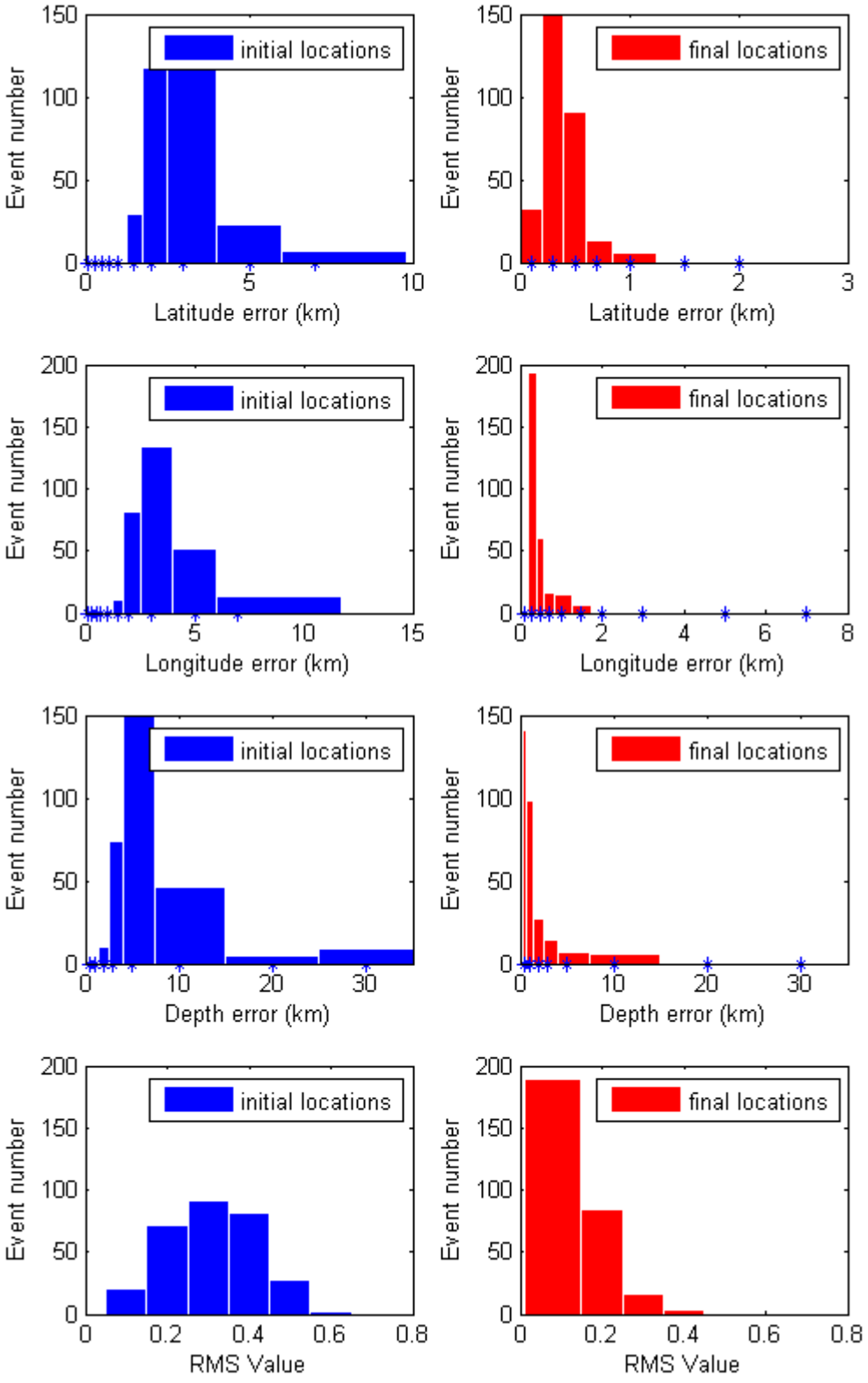

Figure 6.9. Comparison of error in terms of latitude, longitude, depth and RMS for initial and resulting earthquake locations

Figure 6.10 marks the perturbations of the resulting model from 1-D minimum model (Table 6.1).

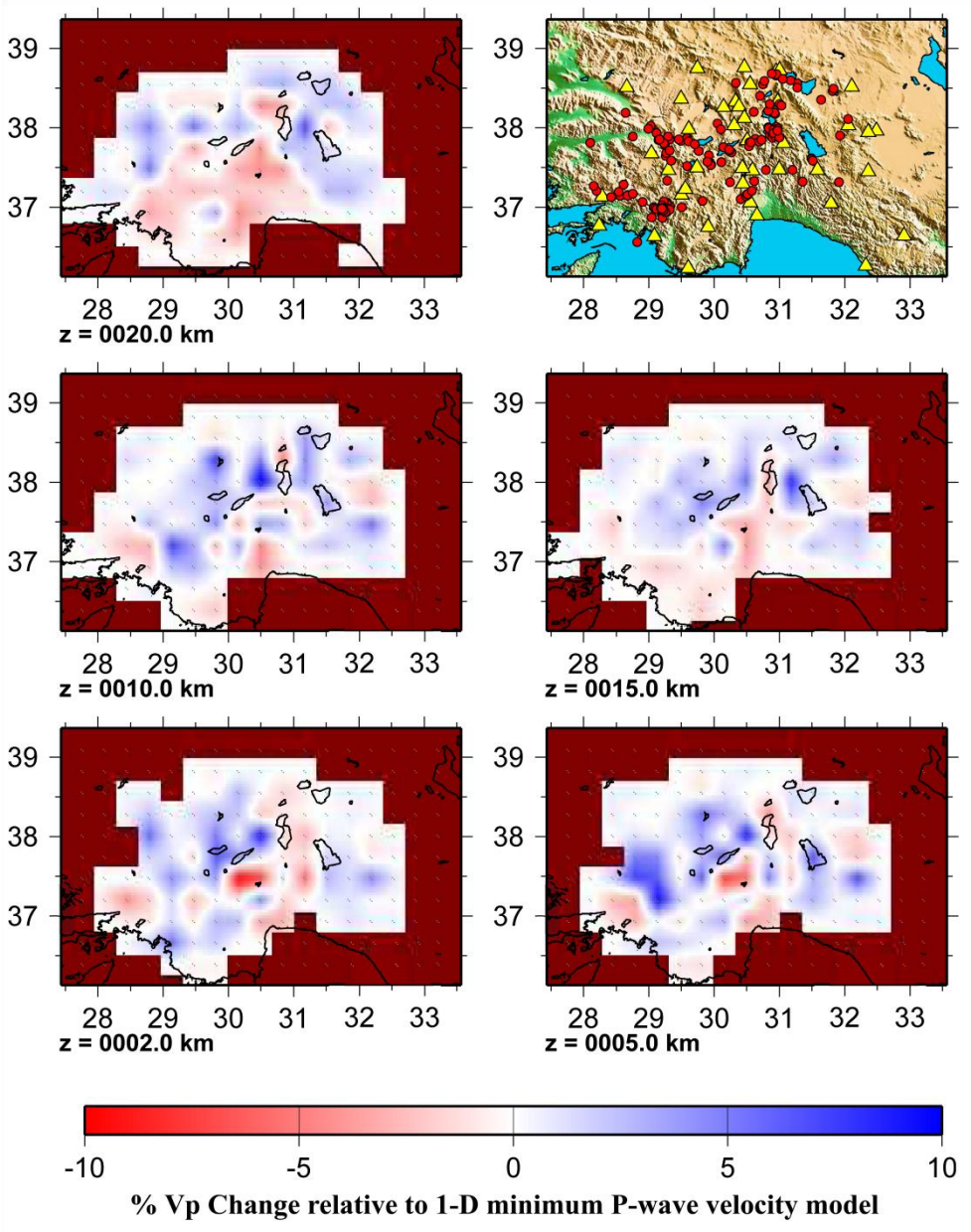

Figure 6.10. Horizontal plane views of Vp perturbations (per cent) relative to the initial 1-D minimum velocity model for different layers down to 20 km. Red circles and yellow triangles represent the events and stations, respectively

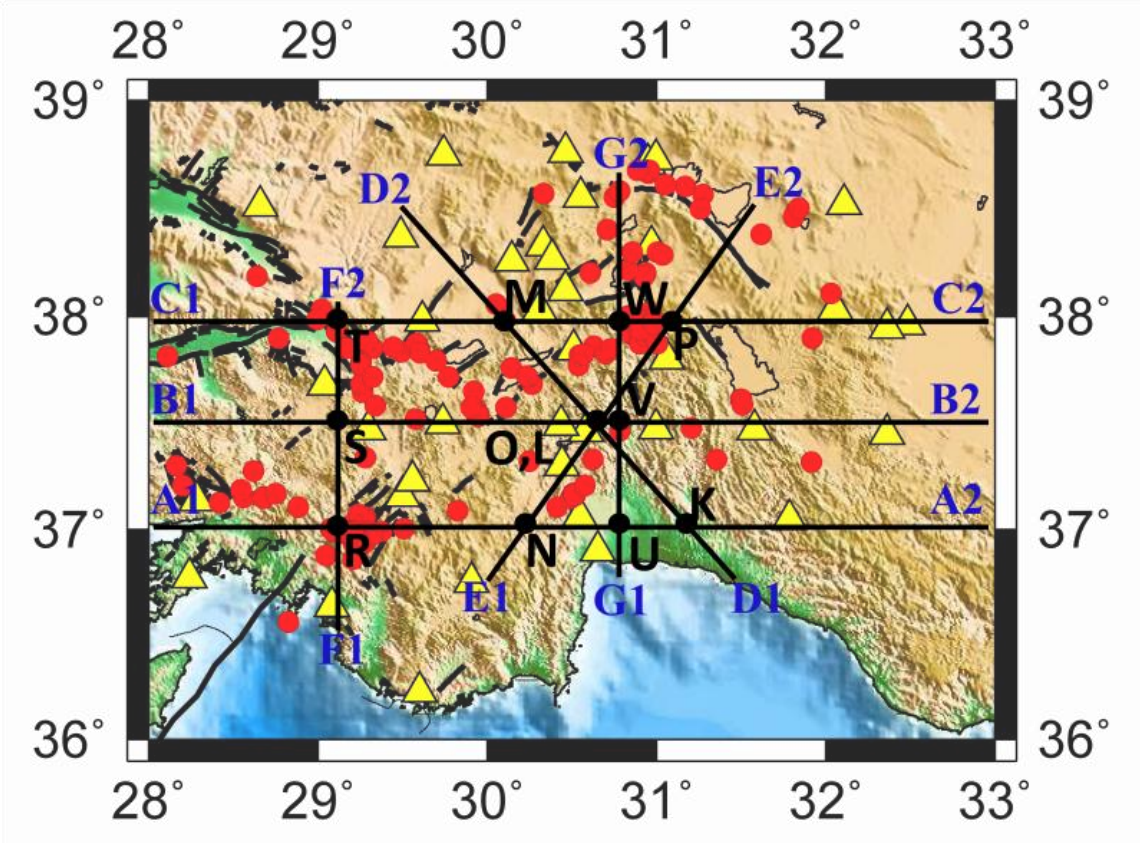

Figure 6.11. Profiles and intersection points

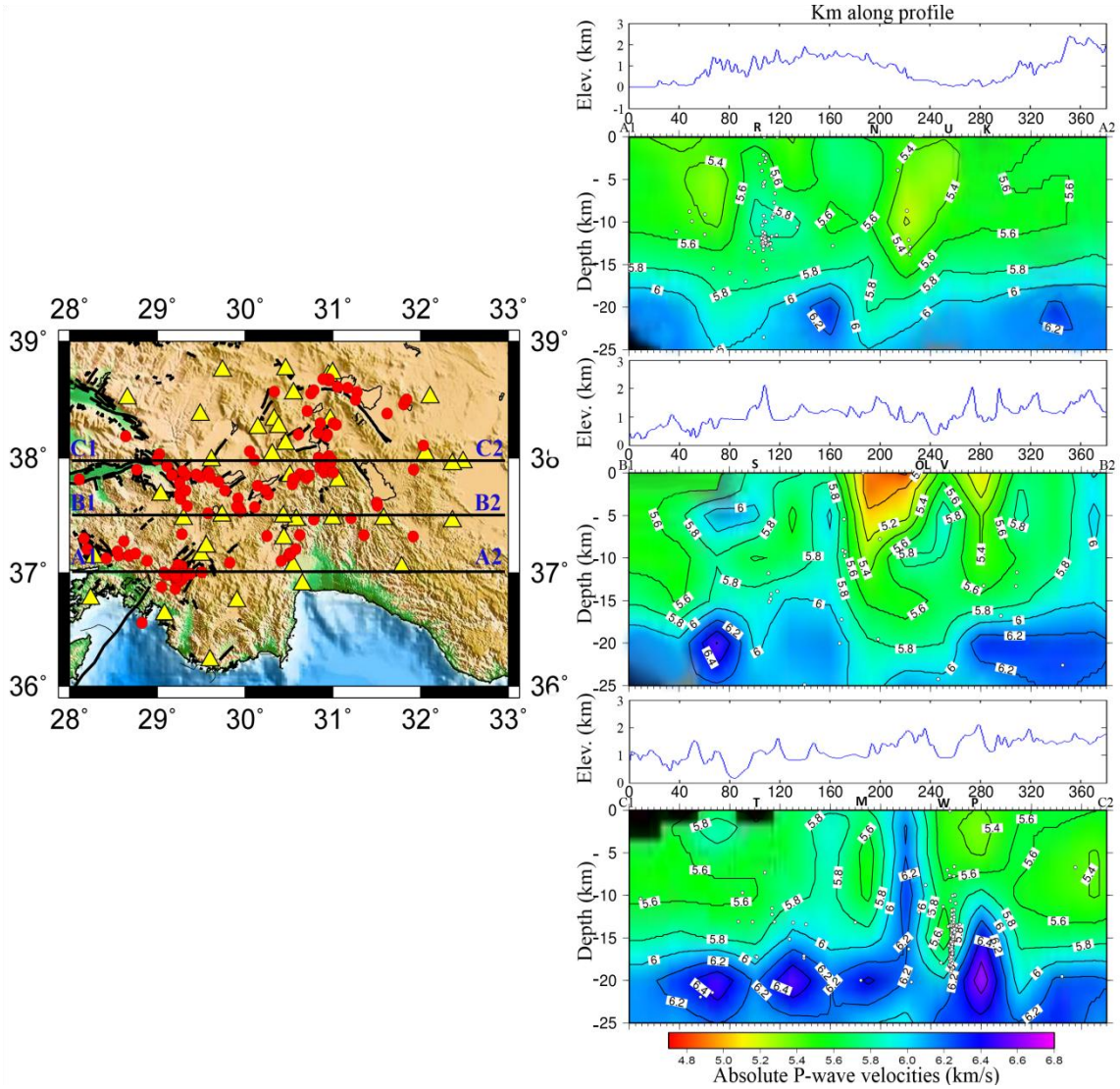

Figure 6.12. P-wave velocity distribution along three profiles (A1-A2 (right up), B1-B2 (right middle), C1-C2 (right down)) for constant latitude values. Yellow triangles denote stations, red and white circles denote earthquake locations

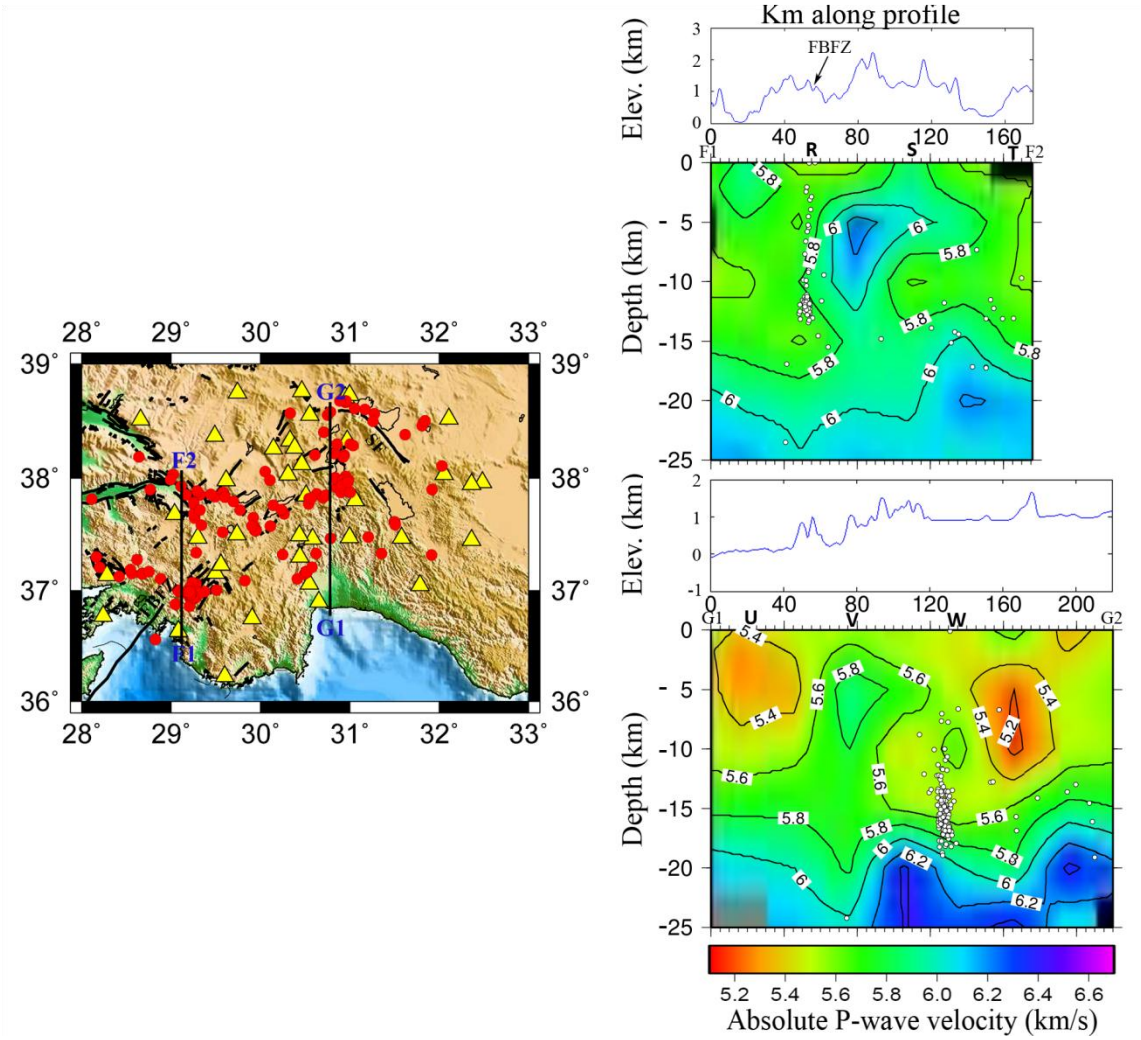

Figure 6.13. P-wave velocity distribution along three profiles (F1-F2 (right up), G1-G2 (right down). Yellow triangles denote stations, red circles denote earthquake locations and white circles denote earthquake locations, FBFZ marks the Fethiye-Burdur-Fault-Zone

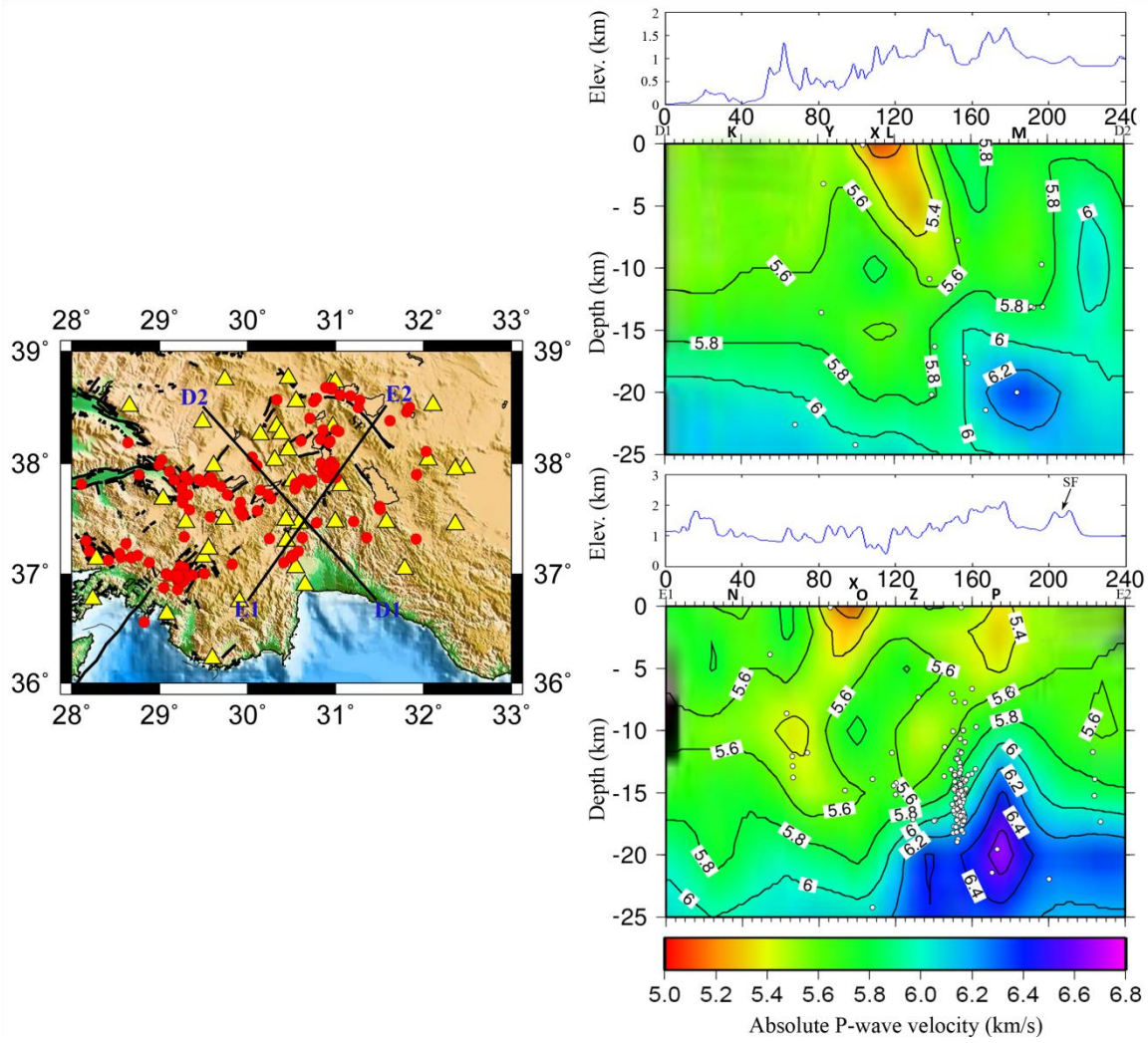

Figure 6.14. P-wave velocity distribution along two profiles (D1-D2 (right up), E1-E2 (right down)). Yellow triangles denote stations, red circles denote earthquake locations and white circles indicate earthquake locations along related profile. SF marks the Sultandağ Fault

Latitude, longitude, depth and RMS errors of initial earthquake locations (Figure 4.1) and final earthquake locations (Figure 6.8) are compared in Figure 6.9. Results show that 3-D P-wave velocity model has a considerable contribution to earthquake location procedure. Profile sections and intersection points are shown in Figure 6.11, intersection points were also shown in profile sections (Figure 6.12, Figure 6.13, and Figure 6.14).

Figure 6.12 displays the constant latitude profile sections of the resulting 3-D P-wave velocity model in the region. As seen on the figure, P-wave velocity from 15 km to 20 km

is reduced from north to south. A relatively low P-wave velocity (5.0 km/s) region for the central part of IA ends surprisingly. As a summary, for the depth from 0 km to 15 km, p-wave velocity decreases from south to north, however it increases for the depth from 15 km to 20 km from south to north.

Figure 6.13 displays the three profile sections, one of which intersects with the Fethiye-Burdur Fault-Zone (FBFZ). The westernmost profile, which cuts across the FBFZ, clearly shows that, profiles has constant velocity (6.0 km/s) below 15 km depth, it has one higher velocity region about the center of profile and 5 km depth. G1-G2 profile, a more seismically active profile, clearly shows that, a region with higher P-wave velocity (6.2 km/s) appears below 20 km depth.

Figure 6.14 shows the P-wave velocity distribution along three profiles. E1-E2 profile is perpendicular to the discontinuity that is called Sultandağ fault. It is clearly seen that there is depth section that has increasing velocity (6.2 km/s – 6.4 km/s) from west to east. This region is located about the center of the region, and 180th km along profile and 20 km depth on both of the two profiles.

7. DISCUSSION AND CONCLUSION

Local earthquake tomography (LET) has become a relatively routine application covered by a dense network. In this research, we built 3-D P-wave velocity model by iterating minimum 1-D P-wave velocity model for the Isparta Angle and surroundings in southwestern Turkey. Data from a two-year (July 2006 - June 2008) field experiment was used to compute 1-D and 3-D P-wave velocity models beneath Isparta Angle and surroundings in southwestern Turkey. The resulting 3-D P-wave velocity model yields high-quality earthquake locations with average location errors of 1 km horizontally. Although 1-D P-wave velocity model can be used to employ earthquake location procedure, 3-D P-wave velocity model can be used in comparative studies. The distribution of seismicity is apparently linked to active faults in the region, notably Fethiye-Burdur-Fault-Zone. Resolution and stability tests demonstrate that 1-D and 3-D P-wave velocity structure for 5-20 km depth is well resolved in this study.

Since the main aim of this study is to resolve the upper crustal model of Isparta Angle and surroundings, local earthquake tomography method has been employed. Isparta Angle and surroundings is an active region in terms of seismicity, however shallow depth earthquakes occur mostly, so the observed phases are mostly the direct arrivals (Pg, Sg), this makes the region compatible to study the LET method. The dense network also makes this region reasonable to study LET method properly.

The use of local earthquakes as sources of seismic arrival time tomography has advantages and disadvantages. Their spatial 3-D distribution makes them feasible to use to determine 3-D velocity model of the crustal structure. However, the lack of control on their distribution and knowledge of their exact locations and origin times are the disadvantages. Compared with the other seismic travel time tomography types, LET can usually offer much higher spatial resolution of structure due to the higher density of ray sampling, higher wave frequency and closer station spacing. The depth extent of LET is limited due to including subsurface events and higher wave frequency.

Priori 1-D P-wave velocity model was generated by using 297 well locatable events, station coordinates and 1-D preliminary P-wave velocity models that have been generated by a trial-error process. This model was improved by combining adjacent layers with similar velocities. 1-D P-wave velocity model and final earthquake locations were used as input to 3-D tomography process. With LET method, the 3-D P-wave velocity structure of upper crust was resolved. Careful analysis of resolution capabilities of the data set demonstrates that the velocity model in central part of Isparta Angle and surroundings is well resolved on a 30x30 km horizontal grid to a depth of about 20 km.

The hypocentral distribution of the events indicates that peak seismicity for the region occurs at depths of about 10 km. The earthquake locations used in this study basically focus on three points. These points are the central part of Fethiye-Burdur-Fault-Zone, the northern tip of Afyon-Akşehir Fault zone and normal faulting zone in the western part of the region. The depth of earthquakes varies from 10 to 20 km. The depth range of the earthquakes illustrates the recent and active deformation zones in the region. There are also other earthquake locations; however the ray density is relatively low for these regions.

Resulting 3-D P-wave velocity model was sampled by profiles across the constant latitudes, profiles that are perpendicular to main discontinuity systems and profiles that cut across earthquake locations that are high in magnitude. E-W oriented depth-cross-sections show that P-wave velocity below the 17 km depth increases from south to north. The western and eastern part of the region display a constant velocity of about 6.2 km/s and central part of the region displays relatively low-velocity material of about 5.8 km/s for specified depth. The subsurface structure below central part of IA displays a constant velocity of about 5.2 km/s, however this region displays higher velocity of about 5.8 – 6.0 km/s on southernmost profile. SW-NW oriented two perpendicular profiles suggest that the shallow subsurface below IA displays a constant velocity of about 5.4 km/s. However the northern part of the IA displays increasing velocity below the 17 km depth. Furthermore, dominant high velocity anomaly was observed along profiles that include the majority of the seismic activities displayed.

Cambaz and Karabulut (2010) declared that relatively low Love-wave velocity for the Isparta Angle and surroundings. Our P-wave velocity results also show a relatively low P-wave velocity anomaly for the region.

Tezel *et al.,* (2010) have found some mid-crustal discontinuities at 10-15 km depths. However we find out a crustal discontinuity below 20 km depth. Regarding the general agreement of Vp/Vs ratio, our velocity anomaly for lower crust is agree with their results.

Glover and Robertson (1998) and Robertson (1993) suggested that, a regional allochthonous unit, Antalya complex, represents a critical part of the evidence of a southern Neotethyan oceanic basin in the central part of IA, our study agrees with this view. Because the subsurface structure below the the central part of IA displays a low P-wave velocity anomaly relatively and this low-velocity material is apparently seen in the resulting P-wave velocity model depth sections and NW-SE (D1-D2 and E1-E2), N-S (G1-G2) and E-W (B1-B2) oriented profiles. Regarding the tectonic structure of the region, this low velocity material may be adressed as the alluvial deposits in central part of IA.

Since Biryol *et al.,* (2011) suggest that dip of the western Cyprus slab at shallow depths (<60 km) beneath Isparta Angle is related to subduction of a locally thicker continental fragment of the African margin, the higher velocity (6.0-6.4 km/s) below the 20 km depth can be inferred as the transition from upper crust to lower crust. Our findings also support Erduran (2009) as he mentioned the thickness of the upper crust is estimated to lie in the range 10–20 km. Our 1-D minimum P-wave velocity model indicates that the region has a crustal thickness about 35 km, which is agree with the result of Kahraman (2008) and Poyraz (2009).

To conclude, tomographic results revealed that there are lateral velocity variations beneath central part of IA and surroundings. Shallow low velocity zones interpreted as alluvium deposits, relatively higher velocity below 20 km depth can be adressed as the transition from upper crust to lower crust. The resolve capability of this study can be improved by using a denser seismic network.

REFERENCES

Aki, K., A. Christoffersson, and E. Husebye, 1976, "Three-dimensional Seismic Structure of the Lithosphere under Montana Lasa", *Bulletin of the Seismological Society of America*, Vol. 66, No. 2, pp. 501-524.

Aki, K., and W.H.K. Lee, 1976, "Determination of Three-dimensional Velocity Anomalies under a Seismic Array Using first P- arrival Time from Local Earthquakes, 1. A Homogeneous Initial Model", *J. Geophys. Res.*, Vol. 81, pp. 4381-4399.

Aki, K., A. Christoffersson, and E. Husebye, 1977, "Determination of Three-dimensional Seismic Structure of the Lithosphere", *Journal of Geophysical Research*, Vol. 82, No. 2, pp. 277-296.

Aksu, A.E., T.J. Calon, J. Hall, S.D. Mansfield, and D. Yaşar, 2005, "The Cilicia–Adana Basin Complex, Eastern Mediterranean: Neogene Evolution of an Active Fore-arc Basin in an Obliquely Convergent Magrin", *Marine Geology*, Vol. 221, pp. 121-159.

Aksu, A.E., J. Hall, and C. Yaltırak, 2005, "Miocene to Recent Tectonic Evolution of the Eastern Mediterranean: New Pieces of the Old Mediterranean Puzzle", *Marine Geology*, Vol. 221, pp. 1-13.

Aktas, K., 2008, *Teleseismic tomography for imaging Earth's upper mantle*, Ph.D. Dissertation, School of Graduate and Postdoctoral Studies University of Western Ontario.

Alcicek, M.C., N. Kazancı, and M. Özkul, 2005, "Multiple Rifting Pulses and Sedimentation Pattern in the Cameli Basin, Southwestern Anatolia", Turkey, *Sedimentary Geology*, Vol. 173, pp. 409-431.

Al-Lazki, A.I., E. Sandvol, D. Seber, M. Barazangi, N. Turkelli, and R. Mohamad, 2004, "Pn Tomographic Imaging of Mantle Lid Velocity and Anisotropy at the Junction of the Arabian, Eurasian and African Plates", *Geophys. J. Int*., Vol. 158, pp. 1024-1040.

Angelier, J., J.F. Dumont, H. Karamanderesi, A. Poisson, Ş. Şimşek, and Ş. Uysal, 1981, "Analyses of Fault Mechanisms and Expansion of Southwestern Anatolia Since the Late Miocene" , *Tectonophysics*, Vol. 75, pp. Tl-T9.

Barka, A., and R., Reilinger, 1997, "Active Tectonics of the Eastern Mediterranean Region: Deduced from GPS, Neotectonic and Seismicity Data", *Annaldi of Geofisica*, Vol. XL, No. 3, pp. 587-610.

Biryol, C.B., S.L., Beck, G., Zandt, and A.A., Özacar, 2011, "Segmented African Lithosphere beneath the Anatolian Region Inferred from Teleseismic P-wave Tomography", *Geophys. J. Int*., Vol. 184, pp. 1037-1057.

Boorder, H., W. Spakman, S.H. White, and W.J.R. Wortel, 1998, "Late Cenozoic Mineralization, Orogenic Collapse and Slab Detachment in the European Alpine Belt", *Earth and Planetary Science Letters*, Vol. 164, pp. 569-575.

Boray, A., and F. Şaroğlu, 1985, "Isparta Büklümünün Kuzey Kesiminde Doğu – Batı Daralma için Bazı Veriler", *MTA Genel Müdürlüğü Jeoloji Mühendisliği*, Vol. Nisan, pp. 9-30.

Bozkurt, E., 2001, "Neotectonics of Turkey – a Synthesis", *Geodinamica Acta*, Vol. 14, pp. 3-30.

Cambaz, M.D., and H. Karabulut, 2010, "Love-wave Group Velocity Maps of Turkey and Surrounding Regions", *Geophys. J. Int*., Vol. 181, pp. 502-520.

Chen, P., L. Zhao, and T.H. Jordan, 2007a, "Full 3D Tomography for the Crustal Structure of the Los Angeles Region", *Bull. Seism. Soc. Am.*, Vol. 97, No. 4, pp. 1094-1120.

Chen, P., L. Zhao, and T.H. Jordan, 2007b, "Full Three-dimensional Tomography: a Comparison between the Scattering-integral and Adjoint-wavefield Methods", *Geophys. J. Int., Vol.* 170, pp. 175-181.

Clayton, R.W., and R.P. Comer, 1983, "A Tomographic Analysis of Mantle Heterogeneities from Body Wave Travel Time (abstract)", Eos, *Trans. Am. Geophys. Union*, Vol. 64, p. 776.

Çoban, H., and M.F.J. Flower, 2006, "Mineral Phase Compositions in Silica-undersaturated-leucite Lamproites from the Bucak Area, Isparta, SW Turkey", *Lithos*, Vol. 89, pp. 275-299.

Dilek, Y., and Ş. Altunkaynak, 2009, "Geochemical and Temporal Evolution of Cenozoic Magmatism in Western Turkey: Mantle Response to Collision, Slab Break-off, and Lithospheric Tearing in a Orogenic Belt", *Geological Society,* Special Publications, London.

Dziewonski, A.M., and D.L. Anderson, 1981, "Preliminary Reference Earth Model", *Phys. Earth Planet. Inter*., Vol. 25, pp. 297-356.

Dziewonski, A.M., and D.L. Anderson, 1984, "Seismic Tomography of Earth's Interior", *Amer. Sci. B*, Vol. 12, pp. 483-494.

Dumont, J.F., A. Poisson, and A. Şahinci, 1979, "Sur l'existence de Coulissements Sinistres Recentes a l'extermite´ Orientale De l'arc Ageen (Sud-ouest de la Turquie)", *C. R. Acad. Sci. Paris 289 Ser. D*, pp. 261-264.

Eberhart-Philips, D., 1986, "Three-Dimensional Velocity Structure in Northwestern California Coast Ranges from Inversion of Local Earthquake Arrival Times", *Bulletin of the Seismological Society of America*, Vol. 76, No. 4, pp. 1025-1052.

Eberhart-Phillips, D., and A.J. Michael, 1993, "Three-dimensional Velocity Structure, Seismicity and Fault Structure in the Parkfield region, Central California", *Journal of Geophysical Research*, Vol. 98, pp. 15737-15758.

Erduran, M., 2009, "Teleseismic Inversion of Crustal S-wave Velocities beneath the Isparta Station", *Journal of Geodynamics*, Vol. 47, pp. 225-236.

Facenna, C., L. Jolivet, C. Primallo, and A. Morelli, 2003, "Subduction and the Depth of Convection in the Mediterranean Mantle", *Journal of Geophysical Research*, Vol. 108, No. B2, pp. 1-13.

Faccenna, C., O. Bellier, J. Martinod, C. Piromallo, and V. Regard, 2006, "Slab Detachment beneath Eastern Anatolia: A Possible Cause for the Deformation of the North Anatolian Fault", *Earth Planet. Sci. Lett*., Vol. 242, pp. 85-97.

Fichtner, A., B.L.N. Kennett, H. Igel, and H.P. Bunge, 2008, "Theoretical Background for Continental and Global Scale Full Waveform Inversion in the Time-frequency Domain", *Geophys. J. Int*., Vol. 175(2), pp. 665-685.

Glover, C., and A. Robertson, 1998, "Neotectonic Intersection of the Aegean and Cyprus Tectonic Arcs: Extensional and Strike-slip Faulting in the Isparta Angle, SW Turkey", *Tectonophysics*, Vol. 298, pp. 103-132.

Gökalp, H., 2007, "Local Earthquake Tomography of the Erzincan Basin and the Surrounding Area in Turkey", *Annals of Geophysics*, Vol. 5, No. 6, pp. 707-724.

Hawley, B.W., G. Zandt, and R.B. Smith, 1981, "Simultaneous Inversion for Hypocenters and Lateral Velocity Variations: An Iterative Solution with Layered Model", *J.Geophys.Res.*, Vol. 86, pp. 7073-7076.

Hirahara, K., 1977, "A Large-scale Three-dimensional Seismic Structure under the Japan Islands and the Sea of Japan", *J. Phys. Earth*, Vol. 25, pp. 393-417.

Husen, S., E. Kissling, and E.R. Flueh, 2000, "Local Earthquake Tomography of Shallow Subduction in North Chile: A Combined Onshoore and Offshoore Study", *J. Geophys. Res.*, Vol. 105, pp. 28183-28198.

Julian, B., J.R. Evans, M.J. Pritchard, and G.R. Foulger, 2000, "A Geometrical Error in Some Computer Programs Based on the Aki-Christofferson-Husebye (ACH) Method of Teleseismic Tomography", *Bulletin of the Seismological Society of America*, Vol. 90, No. 6, pp. 1554–1558.

Kahraman, M., 2008, *Crustal structure of Isparta Angle surrounding regions using P-receiver function analysis*, M.S. Dissertation, Boğaziçi University.

Kahraman, M., N. Turkelli, U.M. Teoman, Ş. Şahin, E.A. Sandvol, and R. Gök, 2010, "Crustal Nature Along the African - Anatolian Collision Zone", *American Geophysical Union Fall Meeting*, 13-17 December 2010, Sanfrancisco, California, USA.

Kalyoncuoğlu, Ü. Y., Ö. Elitok, M.N. Dolmaz, and N.C. Anadolu, 2010, "Geophysical and Geological Imprints of Southern Neotethyan Subduction between Cyprus and the Isparta Angle; SW Turkey", *Journal of Geodynamics*, doi:10.1016/j.jog.2010.12.001.

Kalyoncuoğlu, Ü. Y., and M.F. Özer, 2003, "Determination Of The Crustal Structure Beneath The Isparta Seismograph Station", *Dokuz Eylül Üniversitesi Fen ve Mühendislik Dergisi*, Vol. 5, no.3, pp.111-127.

Kennett, B.L.N., S. Fishwick, A.M. Reading, and N. Rawlinson, 2004, "Contrasts in Mantle Structure Beneath Australia: Relation to Tasman Lines?", *Australian Journal of Earth Sciences*, Vol. 51 (4), pp. 563-569.

Kissling, E., 1988, "Geotomography with Local Earthquake Data", *Rev. Geophys.*, Vol. 26, pp. 659-698.

Kissling, E., W.L. Ellsworth, D. Eberhart-Philips, and U. Kradolfer, 1994, "Initial Reference Models in Seismic Tomography", *J. Geophys. Res*., Vol. 99, pp. 19635-19646.

Kissling, E., U. Kradolfer, and H. Maurer, 1995, "VELEST User's Guide-short Introduction, Report", Inst. of Geophys. and Swiss Seismol. Serv.,Zurich, Switzerland.

Kissling, E., S. Husen, and F. Haslinger, 2001, "Model Parametrization in Seismic Tomography: A Choise of Consequences for the Solution Quality", *Phys.Earth planet.Inter*., Vol. 123, pp. 89-101.

Koulakov, I., T. Stupina, and H. Kopp, 2010, "Case History: Creating Realistic Models Based on Combined Forward Modeling and Tomographic Inversion of Seismic Profiling Data", *Geophysics*, Vol. 75, No. 3, pp. b115-b136.

Le Pichon, X., and J. Angelier, 1979, "The Hellenic Arc and Trench System: A Key to the Neotectonic Evolution of the Eastern Mediterranean Area", *Tectono-physics*, Vol. 60, pp. 1-42.

Lee, W.H.K., and J.C. Lahr, 1975, "A Computer Program for Determining Hypocenter, Magnitude, and First Motion Pattern of Local Earthquakes", *U. S. Geological Survey Open File Report* 75-311, pp. 113.

Lienert, B.R., and J. Havskov, 1995, "A Computer Program for Locating Earthquakes Locally, Regionally and Globally", *Seismological Research Letters*, Vol. 66, pp. 26-36.

Lin, C.H., and S.W. Roecker, 1990, "Determination of Earthquake Hypocenters, Focal Mechanisms, and Velocity Structures in the Morgan Hill Area through 3-D Circular Ray Tracing", *American Geophysical Union*, Vol. 71, No. 43, pp. 1445.

Lippitsch, R., E. Kissling, and J. Ansorge, 2003, "Upper Mantle Structure Beneath the Alpine Orogen from High-resolution Teleseismic Tomography", *Journal of Geophysical Research*, Vol. 108, No. B8.

McKenzie, D., 1972, "Active Tectonics of the Mediterranean Region", *Geophys. J. R. Astron. Soc.*, Vol. 30, pp. 109-185.

McKenzie, D., 1978, "Active Tectonics of the Alpine - Himalayan Belt: The Aegean Sea and the Surrounding", *Geophys. J. R. Astron. Soc.*, Vol. 300, pp. 337-355.

Menke, W., 1989, *Geophysical Data Analysis: Discrete Inverse Theory*, Academic Press, Inc., San Diego.

Mikumo, T., and K. Aki, 1964, "Determination of Local Phase Velocity by Intercomparison of Seismograms from Strain and Pendulum Instruments", *Journal of Geophysical Research*, Vol. 69, pp. 721-731.

Nolet, G., 1985, "Solving or Resolving Inadequate and Noisy Tomographic Systems", *J. Comput. Phys.*, Vol. 61, pp. 463-482.

Nolet, G., 2008, *Global Tomography, A Breviary of Seismic Tomography: Imaging the Interior of the Earth and Sun* , pp. 3-6.

Pavlis, G.L., and J.R. Booker, 1980, "The Mixed Discrete Continuous Inverse Problem: Application to the Simultaneous Determination of Earthquake Hypocenters and Velocity Structure", *J. Gephysics. Res.*, Vol. 85, pp. 4801-4810.

Pavlis, G.L., and J.R. Booker, 1983, "A Study of the Importance of Nonlinearity in the Inversion of Earthquake Arrival Time Data for Velocity Structure", *J. Geophys. Res.*, Vol. 88, pp. 5047-5055.

Poyraz, S.A., 2009, *Isparta Büklümünü Oluşturan Tektonik Yapıların Sismolojik Yöntemlerle Araştırılması,* Ph.D. Dissertation, Istanbul University.

Price, S.P., and B. Scott, 1994, "Fault-block Rotations at the Edge of a Zone of Continental Extension; Southwest Turkey", *Journal of Structural Geology*, Vol. 16, No. 3, pp. 381-392.

Rawlinson, N., and M. Sambridge, 2003, "Seismic Traveltime Tomography of the Crust and Lithosphere", *Andvances in Geophysics*, Vol. 46.

Reilinger, R., 2006, "GPS Constraints on Continental Deformation in the Africa-Arabia-Eurasia Continental Collision Zone and Implications for the Dynamics of Plate Interactions", *Journal of Geophysical Research*, Vol. 111, B05411.

Robertson, A.H.F., 1993, "Mesozoic–Tertiary Sedimentary and Tectonic Evolution of Neotethyan Carbonate Platforms, Margins and Small Ocean Basins in the Antalya Complex, SW Turkey", *Spec. Publ. Int. Assoc. Sedimentol*., Vol. 20, pp. 415–465.

Sapaş, A., and A. Boztepe-Güney, 2008, "Shear Wave Splitting in the Isparta Angle, Southwestern Turkey: Anisotropic Complexity in the Mantle", *J. Earth Syst. Sci*., Vol. 118, No. 1, pp. 71-80.

Sengupta, M.K., and M.N. Toksöz, 1976, "Three Dimensional Model of Seismic Velocity Variation in the Earth's Mantle", *Geophys. Res. Lett*., Vol. 3, pp. 84-86.

Sintubin, M., P. Muchez, D. Simulex-Tohon, G. Verhaert, E. Paulissen, and M. Waelkens, 2003, "Seismic Catastrophes at the Ancient City of Sagalassos (SW Turkey) and Their Implications for Seismotectonics in the Burdur–Isparta Area", *Geological Journal*, Vol. 38, pp. 359-374.

Teoman, U.M., 2005, *3-D P-wave Velocity Structure Beneath Eastern Turkey Applying Local Earthquake Tomography (LET) Method*, M.S. Dissertation, Boğaziçi University.

Tezel, T., T. Shibutani, and B. Kaypak, 2010, "Crustal Structure Variation in Western Turkey Inferred from the Receiver Function Analysis", *Tectonophysics*, Vol. 492, pp. 240-252.

Thurber, C.H., 1983, "Earthquake Locations and Threee Dimensional Crustal Velocity Structure in the Coyota Lake Area, Central California", *J. Geophys. Res*, Vol. 88, pp. 8226-8236.

Thurber, C.H., 1992, "Hypocenter-velocity Structure Coupling in Local Earthquake Tomography", *Phys. Earth Planet. Inter.*, Vol. 75, pp. 55-62.

Thurber, C.H., 1993, *Seismic Tomography*, Chapman and Hall, London, pp. 563-583.

Thurber, C.H., and D. Eberhart-Philips, 1999, "Local Earthquake Tomography with Flexible Gridding", *Computers & Geosciences*, Vol. 25, pp. 809-818.

Toomey, D.R., and G.R. Foulger, 1989, "Tomographic Inversion of Local Earthquake Data from the Hengill-Grensdalur Central Volcano Complex, Iceland", *Jour. Geophys. Res*., Vol. 94, pp. 497–510.

Udias, A., 1999, *Principles of seismology*, Cambridge University Press, pp. 260

Um, J., and C.H. Thurber, 1987, "A Fast Algorithm for Two-point Seismic Ray Tracing", *Bull. Seismol. Soc. Am*, Vol. 77, pp. 972-986.

Veen, J., 2004, "Extensions of Hellenic Forearc Shear Zones in SW Turkey: the Pliocene Quaternary Deformation of the Eşen Çay Basin", J. *Geod*., Vol.37, pp. 181-204.

Virieux, J., and V. Arra, 1991, "Ray Tracing in 3-D Complex Isotrophic Media: An Analysis of the Problem", *Geophysics*, Vol. 59, pp. 2057-2069.

Waldhauser, F., R. Lippitsch, E. Kissling, and J. Ansorge, 2002, "High-resolution Teleseismic Tomography of Upper Mantle Structure Using a Priori 3D Crustal Model", *Geophys. J. Int*., Vol. 150, pp. 141–403.

Yağmurlu, F., Y. Savaşçın, and M. Ergün, 1997, "Relation of Alkaline Volcanism and Active Tectonism within the Evolution of Isparta Angle", SW Turkey, *Journal of Geology*, Vol. 105, pp. 717-728.

Yağmurlu, F., and M. Şentürk, 2005, "Güneybatı Anadolu'nun Güncel Tektonik Yapısı", *Türkiye Kuvaterner Sempozyumu*, Türkiye, 2-5 Haziran 2005, İstanbul Teknik Üniversitesi Avrasya Yer bilimleri Enstitüsü.

Yang, T., and Y. Shen, 2005, "P-wave Velocity Structure of the Crust and Uppermost Mantle beneath Iceland from Local Earthquake Tomography", *Earth and Planetary Science Letters*, Vol. 235, Issue. 3-4, pp. 597-609.

Yoshizawa, K., and B.L.N. Kennett, 2004, "Multi-mode Surface Wave Tomography for the Australian Region Using a Three-stage Approach Incorporating Finite Frequency Effects", *J. Geophys. Res*., Vol. 109, B02310.

Zhao, D., S. Todo, and J. Lei, 2005, "Local Earthquake Reflection Tomography of the Landers Aftershock Area", *Earth and Planetary Science Letters*, Vol. 235, pp. 623–663.